

## Article

# Inverse Analysis of Structural Damage Based on the Modal Kinetic and Strain Energies with the Novel Oppositional Unified Particle Swarm Gradient-Based Optimizer

Nizar Faisal Alkayem <sup>1,2</sup> , Lei Shen <sup>3</sup>, Tareq Al-hababi <sup>4</sup> , Xiangdong Qian <sup>4</sup>  and Maosen Cao <sup>4,\*</sup><sup>1</sup> College of Civil and Transportation Engineering, Hohai University, Nanjing 210098, China<sup>2</sup> The Anhui Provincial International Joint Research Center of Data Diagnosis and Smart Maintenance on Bridge Structures, Chuzhou University, Chuzhou 239000, China<sup>3</sup> College of Water Conservancy and Hydropower Engineering, Hohai University, Nanjing 210098, China<sup>4</sup> Department of Engineering Mechanics, Hohai University, Nanjing 210098, China

\* Correspondence: cmszhy@hhu.edu.cn

**Abstract:** Structural damage inspection is a key structural engineering technique that strives for ensuring structural safety. In this regard, one of the major intelligent approaches is the inverse analysis of structural damage using evolutionary computation. By considering the recent advances in this field, an efficient hybrid objective function that combines the global modal kinetic and modal strain energies is introduced. The newly developed objective function aims to extract maximum dynamic information from the structure and overcome noisy conditions. Moreover, the original methods are usually vulnerable to the associated high multimodality and uncertainty of the inverse problem. Therefore, the oppositional learning (OL) for population initialization and convergence acceleration is first adopted. Thereafter, the unified particle swarm algorithm (UPSO) mechanism is combined with another newly developed algorithm, the gradient-based optimizer (GBO). The new algorithm, called the oppositional unified particle swarm gradient-based optimizer (OL-UPSGBO), with the convergence acceleration feature of (OL), enhances balanced exploration-exploitation of UPSO, and the local escaping operator of GBO is designed to specifically deal with the complex inverse analysis of structural damage problems. To authenticate the performance of the OL-UPSGBO, the complex benchmark set of CEC 2017 is adopted to compare the OL-UPSGBO with several original metaheuristics. Furthermore, the developed approach for structural damage identification is tested using several damage scenarios in a multi-story frame structure. Results show that the developed approach shows superior performance and robust behavior when tackling the inverse analysis of structural damage.

**Keywords:** inverse analysis; structural damage identification; modal kinetic energy; modal strain energy; evolutionary algorithms; soft computing



**Citation:** Alkayem, N.F.; Shen, L.; Al-hababi, T.; Qian, X.; Cao, M. Inverse Analysis of Structural Damage Based on the Modal Kinetic and Strain Energies with the Novel Oppositional Unified Particle Swarm Gradient-Based Optimizer. *Appl. Sci.* **2022**, *12*, 11689. <https://doi.org/10.3390/app122211689>

Academic Editors: Antonio J. Nebro and José Manuel García-Nieto

Received: 20 September 2022

Accepted: 9 November 2022

Published: 17 November 2022

**Publisher's Note:** MDPI stays neutral with regard to jurisdictional claims in published maps and institutional affiliations.



**Copyright:** © 2022 by the authors. Licensee MDPI, Basel, Switzerland. This article is an open access article distributed under the terms and conditions of the Creative Commons Attribution (CC BY) license (<https://creativecommons.org/licenses/by/4.0/>).

## 1. Introduction and Literature Review

Structural health monitoring (SHM) has gained great significance in the last decade due to well-founded signal processing developments, vibration engineering, computational intelligence, etc. Moreover, the SHM methods have gained more attention by the research community due to its role in guaranteeing structure safety and severability [1,2]. Efficient SHM systems permit precocious detection of structural damage through non-destructive testing, data analysis, and modal feature analysis in order to prevent structural failure [3,4]. Major SHM methods [5] include, but are not limited to, inverse analysis, model updating, machine learning, probabilistic and deterministic approaches, metaheuristics, etc. Nevertheless, due to the high uncertainty, as well as environmental and loading effects, associated with damage inspection, it is impossible to achieve a “one fits

all” method for all SHM applications; in addition to the various different types of civil structures being tested, such as frames, beams, bridges, buildings, dams, etc., or mechanic structures, such as rotary machines, aeronautical structures, trains, vehicles, etc. [6–8]. Modern damage detection techniques mainly rely on data-driven methods which focus on detecting the existence of damage and identifying the relative location of it. Other modern approaches depend on model-based inverse problems, for which the FE model updating is implemented. FE model updating is conducted to identify damage location and severity by means of finding the correlation between numerical and experimental modal responses. Thereafter, the FE model is altered to match the real situation of the structure. This approach will be the main focus of this work.

Vibration modal characteristics are main structural parameters that are utilized for the inverse analysis of structural damage [9,10]. Such characteristics are mainly categorized into modal frequencies, modal shapes, curvature modal shapes, strain energy, flexibility, kinetic energy, etc. In this regard, researchers often implement single or multiple modal features in their attempts to develop efficient and robust paradigms able to tackle the model-based damage diagnosis problem. The basic idea of solving the inverse problem of model-based damage identification is to construct an optimization problem, in which the error between the measured responses and analytical responses is taken from the FE model [11,12]. Therefore, by using the modal features [13], the objective function of the inverse problem is developed. An overview of modal-features-based objective functions available in the literature is provided in the following section.

The inverse analysis of structural damage identification problems involves two important aspects. The first aspect to be addressed is the formulation of the objective function, which measures the difference between the responses of the FE model of the initial state of the structure and the real responses corresponding to the current situation of the structure experiencing damage [5,14–16]. Modal strain energy (MSEn) is one of the most useful modal features that can be used to formulate the objective function. It has proved to be more accurate in detecting minor damage than other modal features, such as natural frequencies and mode shapes [17,18]. Therefore, the MSEn is utilized as a damage index to detect and localize structural damage. Several studies have employed MSEn damage indicators in bridge structures [19], plates [20], trusses and frames [21], beams [22], etc. Most studies have reported the effective damage identification capabilities of MSEn when applied on different structures, even under conditions that lack complete data or have noisy responses. The second aspect to be addressed, modal kinetic energy (MKEn), is another effective modal characteristic that can be used as an informative indicator of structural damage. Very few research studies have implemented the MKEn for damage identification. For example, Dinh-Cong et al. [23] proposed a multi-stage damage detection of truss structures, in which the MKEn is firstly implemented to discover possible damage locations, and then a model updating approach using hybrid flexibility and mode shapes objective function with the symbiotic organisms search for accurate damage identification. In their other work, Dinh-Cong et al. [24] implemented MKEn-based sensitivity for the successful damage identification in composite beams. Joseph et al. [25,26] also used the sensitivity of MKEn for damage identification in 2D simple supported beams. Pooya et al. [27] developed a new damage identification index based on the relative differences of MSEn and MKEn, particularly for beam-like structures. Additionally, Torkzadeh et al. [28] developed a two-stage damage identification approach in which the MKEn is first used for initial assessment of structural damage, whereas the MSEn is later used to formulate an objective function that was solved by PSO algorithm. Results showed successful damage identification in truss structures. Xu et al. [29] proposed a cross modal sensitivity of MSEn and MKEn for damage identification in beam and offshore platform structures. Another research work was conducted by Shahri and Ghorbani-Tanha [30], in which the sensitivity of MKEn was utilized for damage identification in simple supported beams. From the aforementioned literature review, it can be concluded that the MKEn is a useful damage indicator that can be used for the inverse problem of SHM. Nevertheless, it has rarely been

used in research. Moreover, it has not been explicitly used as the main objective function within the inverse problem of structural damage identification, and has only been used as a damage indicator for localizing possible damage in structures. Therefore, it is very useful to use the MKEn and integrate it with MSEN to formulate an efficient objective function that can extract maximum damage information from structures.

In order to solve the inverse analysis of structural damage identification, soft computing techniques have been widely used [31]. In particular, the recent advances in evolutionary computation have boosted soft computing techniques into more practical applications, due to their robust foundation and high computational abilities. Evolutionary computation involves various algorithms that mimic several nature processes, such as evolutionary theory [32], physics-based phenomena [33], herding and breeding behaviors of creatures [34,35], swarm-based behavior [36], etc. Such algorithms are highly recommended for solving inverse problems; i.e., the problem of inverse analysis of structural damage. Several representative research studies have been reported. For example, Ghannadi and Kourehli [37] tested the efficiency of slime mold optimization for structural damage identification in various case studies. In other studies, conducted by the same authors, the gray wolf optimizer (GWO) was successfully utilized for similar case studies [38], as well as the multi-verse optimizer (MVO) [39]. Gomes and Giovani [40] developed a two-stage damage identification method using the sunflower optimization algorithm for application to plate structures. Moreover, Pereira et al. [41,42] studied the efficiency of the Lichtenberg optimization algorithm for structural damage identification in plate structures. Khatir et al. [43] compared several algorithms for the purposes of damage identification in truss structures. In other studies, conducted by the same research group, several evolutionary algorithms were used, such as the hybrid evolutionary-neural network approach [44], the modified PSO algorithm in [45], and the improved velocity strategy PSO in [46], etc. Kaveh et al. [47] developed the plasma generation algorithm for damage detection in truss structures. Similarly, other research studies have been conducted by Kaveh et al. [48,49] for the same purpose. Other new research studies were observed in [50–52]. Among the novel evolutionary computation methods, the gradient-based optimizer (GBO) is a newly introduced MH for solving numerical optimization problems [53]. It mainly involves the stochastic conversion of gradient theory into a population-based optimization algorithm. The main mathematical proposal of GBO is to modify the Newtonian gradient method using an evolutionary paradigm with the innovative local-escaping mechanism for overcoming complex optimization problems. Therefore, it is important to explore the performance of GBO to solve the inverse analysis of structural damage problems in addition to boosting its search mechanism to make it more suitable to overcome complex computational tasks associated with the inverse analysis of assessment of structural damage. Hence, the GBO is improved by using two search mechanisms. First, oppositional-based learning (OL), which is a powerful optimization assistant tool that evaluates the oppositional of a considered solution and compares the two solutions in order to choose a better one. This efficient tool can help to accelerate the convergence of the algorithm and explore more search areas, which suits problems with multimodality and multiple local optima, such as the problem of structural damage assessment. In addition, the local search mechanism of a powerful PSO variant, the unified PSO (UPSO), can also be incorporated with the main computational framework of GBO to boost the local search ability of GBO and provide accelerated performance to deal with the high computational problem of the inverse analysis of structural damage. Therefore, another major contribution of this article is to design, test, and verify a new optimization algorithm called the oppositional unified particle swarm gradient-based optimizer (OL-UPSGBO), which is specifically designed to overcome the complex optimization problem of the inverse analysis of structural damage.

The main contributions of this study can be summarized as: (i) a new hybrid objective function that mainly depends on modal kinetic and strain energies for the problem of inverse analysis of structural damage is introduced; (ii) a new optimization algorithm called the OL-UPSGBO, which incorporates the OL, the UPSO, and the GBO, is devel-

oped; (iii) the new algorithm is first tested and verified using the most challenging benchmark function set, which is the Congress of Evolutionary Algorithms (CEC-2017) and it is compared and verified against some recently developed evolutionary algorithms; (iv) the framework of structural damage assessment is introduced and case studies are presented using incomplete and noisy modal responses.

The rest of this study is divided into the following sections: (i) Section 2 presents the theoretical background of the problem of inverse analysis of structural damage, as well as the development of the new hybrid objective function; (ii) the novel OL-UPSGBO is introduced in Section 3 and verification experiments are presented; (iii) the total structural damage identification framework and case studies, as well as the results of the case studies including the overall challenges, achievements, and recommendations are discussed in Section 4; (iv) the concluding remarks and future scope are presented in Section 5.

## 2. Theory of the Inverse Analysis of Structural Damage

### 2.1. The Model-Based Inverse Method for Structural Damage Identification

Inverse problems in structural mechanics are well-known frameworks for structural damage identification. The underlying assumption can be described as being when damage occurs in a structure and its features are output responses. This can be represented as  $f_{output} = (f_1, f_2, \dots, f_m)$ , in which response functions are selected for particular purposes and an optimization problem is formulated; where  $m$  is the number of possible extracted features from the structure. The optimization problem should be developed with corresponding features to reflect the changes in the structure in comparison with the original intact structure. The updated damage parameters related to  $n$  elements  $\alpha = (\alpha_1, \alpha_2, \dots, \alpha_n)$ , which represent the damage occurred in the structural elements, are the parameters of the function of the input  $f_{output} = (\alpha_1, \alpha_2, \dots, \alpha_n)$ . The target of the optimization problem is to confirm whether the parameter vector  $\alpha$  matches the current situation of the structure or not. So, when we update the model, the final outcomes obtained from finite element analysis are consistent with the known real  $f_{output}$  of the damaged structure. Tracking the values of  $\alpha$  requires an appropriate objective function and that its characteristics are linked to the updating parameters  $\alpha = (\alpha_1, \alpha_2, \dots, \alpha_n)$ . Hence, the objective function is a vital factor for tracking the correct vector  $\alpha = (\alpha_1, \alpha_2, \dots, \alpha_n)$ . As was observed in the literature review section, several features have been developed in the field of structural damage identification, and it is impossible to choose a “one fits all” objective function. Moreover, the inverse problem is a multi-stage mathematical problem in which the link between  $\alpha$  and  $f_{output}$  is indirect and contains a multiplication of large vectors and matrices, which makes the exact physical description difficult to comprehend. Additionally, the use of stochastic algorithms to solve the inverse problem makes the overall process a black box. In the next section, this work will introduce a novel combined objective function, which is designed to incorporate three modal features that are able to extract the most possible damage information from the structure.

### 2.2. Proof of the Principle of Damage Identification (Sensitivity Analysis)

As has been shown in the literature review, there are very few studies that implement MKEn for inverse analysis of structural damage; MSEN is more widely used as a main structural damage detection indicator, due to its direct link to the stiffness matrix of the structure. Nevertheless, due to the concept of energy conversion, both MKEn and MSEN mutually transform between each other, which makes them both highly sensitive to the occurrence of structural damage, particularly when stiffness alterations due to damage exist. In this regard, the derivation of MKEn and MSEN change ratios are presented in order to formulate the objective function necessary for the inverse problem of structural damage identification [9–12,24,30].

The sensitivity analysis is first conducted on the MKEn to proof its sensitivity for damage when the change is made in Young's modulus of elasticity to explain the rate of change in MKEn when implementing a minor perturbation in the system.

In structural dynamics, the free vibration of the FE model of the structure with  $N_m$  degrees of freedom, the following equation can be written as:

$$[K]\{\phi_i\} = \omega_i[M]\{\phi_i\}, \tag{1}$$

where  $[K]$  and  $[M]$  are the  $N_m \times N_m$  global stiffness and mass matrices of the structure, respectively;  $\{\phi_i\}$  and  $\omega_i$  are mode shape and modal frequencies of the  $i$ th mode of vibration, respectively.

According to continuous damage mechanics, and due to various internal and external conditions surrounding the structure, damage occurs and in turn alters the free vibration equation, which can be expressed by a scalar variable  $\alpha_j = (\alpha_1, \alpha_2, \dots, \alpha_n)$  corresponding to  $n$  number of elements and  $\alpha_j \in [0, 1]$ . As the damage might occur in some elements, then, by discretizing the model, the global stiffness and mass matrices can be formulated by the scalar multiplication of the elemental matrices and damage parameters; hence, the global stiffness and mass matrices after damage can be written as:

$$[K]^D = \sum_{j=1}^n \alpha_j [K]_j, \tag{2}$$

and

$$[M]^D = \sum_{j=1}^n \alpha_j [M]_j, \tag{3}$$

where the superscript  $D$  refers to the damage of the structure;  $[K]_j$  and  $[M]_j$  are the element stiffness and mass matrices of the  $j$ th element of the structure;  $n$  is the total number of elements.

From the theory of modal energy, the global  $MKE_n$  of the intact structure and the  $MKE_n^D$  of the damaged structure can be derived from the mode shapes and the stiffness matrix of the structure as:

$$MKE_n = \frac{1}{2} \omega_i \{\phi_i\}^{Tr} [M]_j \{\phi_i\}, \tag{4}$$

and

$$MKE_n^D = \frac{1}{2} \omega_i^D \{\phi_i^D\}^{Tr} [M^D]_j \{\phi_i^D\}. \tag{5}$$

where the superscript  $Tr$  refers to the transpose. As noted in [24], when damage occurs in a structure, the ratio of change of  $MKE_n$  in each element can serve as a damage indicator, as:

$$MKE_n R_{ij} = \frac{\Delta MKE_{n_{ij}}}{MKE_{n_{ij}}} = \frac{MKE_{n_{ij}}^D - MKE_{n_{ij}}}{MKE_{n_{ij}}}. \tag{6}$$

The sensitivity of  $MKE_n$ , with respect to a damage parameter  $p$ , which can be any physical parameter such as Young's modulus, mass density, etc. [24,30], can be written as:

$$\frac{\partial MKE_{n_{ij}}}{\partial p} = \frac{1}{2} \left( \frac{\partial \omega_i}{\partial p} \{\phi_i\}^{Tr} [M]_j \{\phi_i\} + \omega_i \{\phi_i\}^{Tr} \frac{\partial [M]_j}{\partial p} \{\phi_i\} + 2\omega_i [M]_j \frac{\partial \{\phi_i\}}{\partial p} \right). \tag{7}$$

It is assumed that damage has only occurred due to the reduction of Young's modulus (i.e., reduction in stiffness). Therefore, it is assumed that no mass change has occurred in the structure, and Equation (7) can be written as:

$$\frac{\partial MKE_{n_{ij}}}{\partial p} = \left[ 2\omega_i [M]_j \quad \frac{1}{2} \{\phi_i\}^{Tr} [M]_j \{\phi_i\} \right] \begin{Bmatrix} \frac{\partial \{\phi_i\}}{\partial p} \\ \frac{\partial \omega_i}{\partial p} \end{Bmatrix}. \tag{8}$$

The second vector, which is the first order derivative of the modal parameters, is derived and can be further studied in references [24,30] as:

$$\begin{Bmatrix} \frac{\partial\{\phi_i\}}{\partial p} \\ \frac{\partial\omega_i}{\partial p} \end{Bmatrix} = \begin{bmatrix} [K] - \omega_i[M] & -[M]\{\phi_i\} \\ -\{\phi_i\}^T[M] & 0 \end{bmatrix} \begin{Bmatrix} -\left(\frac{\partial[K]}{\partial p_i} - \omega_i \frac{\partial[M]}{\partial p}\right)\{\phi_i\} \\ \frac{1}{2}\{\phi_i\}^T \frac{\partial[M]}{\partial p} \{\phi_i\} \end{Bmatrix}. \tag{9}$$

By substitution of Equation (9) into Equation (10), the MKE sensitivity of *j*th element for *i*th mode of vibration will be as:

$$\frac{\partial MKEn_{ij}}{\partial p} = \{\phi_i\}^T [\omega_i[M]_j \quad \frac{1}{2}[M]_j\{\phi_i\}] [K_{U/D}]^{-1} [F_p] \{\phi_i\}. \tag{10}$$

In which

$$K_{U/D} = \begin{bmatrix} [K] - \omega_i[M] & -[M]\{\phi_i\} \\ -\{\phi_i\}^T[M] & 0 \end{bmatrix}, \tag{11}$$

and

$$F_p = \begin{bmatrix} -\left(\frac{\partial[K]}{\partial p_j} - \omega_i \frac{\partial[M]}{\partial p}\right) \\ \frac{1}{2}\{\phi_i\}^T \frac{\partial[M]}{\partial p} \end{bmatrix}, \tag{12}$$

where the subscript *U/D* refers to the undamped system with distinct and well-spaced natural frequency. The parameter *p<sub>i</sub>* is the physical parameter that is used to calculate the elemental mass and stiffness matrices. By assuming that for the *i*th element there is a corresponding parameter *p<sub>i</sub>* which can be considered to be the Young’s modulus of elasticity or mass density, or any other parameter of interest. In most of the vibration-based damage identification approaches, it is assumed that the mass matrix of the structure will not change due to the occurrence of damage. Hence, the parameter *p<sub>i</sub>* is assumed to be the Young’s modulus of elasticity. This assumption involves only the stiffness changes of the system and limits the mass change of the structure to zero. Therefore, the sensitivity matrix of MKEn with respect to parameter *E<sub>i</sub>* is written as:

$$\frac{\partial MKEn_{ij}}{\partial E_j} = \{\phi_i\}^T [\omega_i[M]_j \quad \frac{1}{2}[M]_j\{\phi_i\}] [K_{U/D}]^{-1} [F_{E_j}] \{\phi_i\}, \tag{13}$$

where  $F_p = \begin{bmatrix} -\frac{\partial[K]}{\partial p} \\ 0 \end{bmatrix}$ .

Using the first order Taylor series expansion, the ratio of change of MKEn can be written as:

$$\Delta MKEn_{ij} = \sum_{j=1}^n \frac{\partial MKEn_{ij}}{\partial E_i} \Delta E_j, \tag{14}$$

and the ratio of change of [K] can be written as:

$$[\Delta K] = \sum_{j=1}^n \frac{\partial[K]}{\partial E_j} \Delta E_j, \tag{15}$$

To calculate the matrix variation [ΔK], which describes the global stiffness matrix change between the intact and healthy structure, the global stiffness matrix should be calculated using the assembly of the elemental stiffness matrix that indicates damage in each element. Hence, the [ΔK] can be calculated as:

$$[\Delta K] = [K] - [K]^D = \sum_{j=1}^n \alpha_j [K]_j, \quad (0 \leq \alpha_j \leq 1). \tag{16}$$

The alpha parameter in the above equation indicates the severity of damage. The zero value indicates no damage, and the value of one indicates a full damage corresponding to the  $j$ th element.

By multiplying Equation (10) by the  $\Delta E_j$  and summing up for all  $E_j$ , it yields:

$$\Delta MKEn_{ij} = \{\phi_i\}^T [\omega_i[M]_j \quad \frac{1}{2}[M]_j\{\phi_i\}] [K_{U/D}]^{-1} \begin{bmatrix} -\sum_{j=1}^n \alpha_j [K]_j \\ 0 \end{bmatrix} \{\phi_i\}, \tag{17}$$

Equation (17) can be simplified to:

$$\Delta MKEn_{ij} = \sum_{j=1}^n \alpha_j \{\phi_i\}^T [s]_j \{\phi_i\}, \tag{18}$$

where

$$[s]_j = [\omega_i[M]_j \quad \frac{1}{2}[M]_j\{\phi_i\}] [K_{U/D}]^{-1} \begin{bmatrix} -[K]_j \\ 0 \end{bmatrix}. \tag{19}$$

Finally, by using Equation (6), MKEnR sensitivity matrix  $[S^*]_{i,r}$  can be obtained by

$$[s^*]_k = \frac{1}{\frac{1}{2}\omega_i\{\phi_i\}^T [M]_j\{\phi_i\}} [\omega_i[M]_j \quad \frac{1}{2}[M]_j\{\phi_i\}] [K_{U/D}]^{-1} \begin{bmatrix} -[K]_k \\ 0 \end{bmatrix}. \tag{20}$$

Hence, Equation (17) can be simplified as:

$$[s^*]\{\alpha\} = \{\Delta R\}, \tag{21}$$

where

$$\Delta R_{ij} = MKEnR_{ij}, \text{ and} \\ S_{kij}^* = \sum_{j=1}^n \alpha_j \frac{1}{\frac{1}{2}\omega_i\{\phi_i\}^T [M]_j\{\phi_i\}} [\omega_i[M]_j \quad \frac{1}{2}[M]_j\{\phi_i\}] [K_{U/D}]^{-1} \begin{bmatrix} -[K]_k \\ 0 \end{bmatrix}. \tag{22}$$

In the abovementioned description, the MKEnR sensitivity of the  $j$ th element to specific change in  $k$ th member's Young's modulus of elasticity for the  $i$ th mode of vibration has been achieved. Additionally,  $\Delta R_{ij}$  is the MKEnR in the  $j$ th element for the  $i$ th mode of vibration. For further information, references [24,30] can be referred to.

Based on the above mathematical derivation, it is clear that the modal kinetic energy is sensitive to damage occurrence, even when only the Young's modulus is responsible for the damage phenomenon in the structure with an absence of mass change.

Similar to the aforementioned mathematical derivations related to the sensitivity of the MKEn modal feature to damage, a similar analysis should be conducted for the MSEN modal feature. Again, from the theory of modal energy, the global  $MSEn$  of the intact structure and the  $MSEn^D$  of the damaged structure can be derived from the mode shapes and the stiffness matrix of the structure as:

$$MSEn = \frac{1}{2} \{\phi_i\}^T [K] \{\phi_i\}, \tag{23}$$

and

$$MSEn^D = \frac{1}{2} \{\phi_i^D\}^T [K^D] \{\phi_i^D\}, \tag{24}$$

As pointed out in [20,21], when damage occurs in a structure the ratio of change of MSEN in each element can serve as a damage indicator, as:

$$MSEnR_{ij} = \frac{\Delta MSEn_{ij}}{MSEn_{ij}} = \frac{MSEn_{ij}^D - MSEn_{ij}}{MSEn_{ij}}. \tag{25}$$

The derivative of Equation (4) in respect to  $p$  is:

$$\frac{\partial MSEN_{ij}}{\partial p} = \frac{1}{2} \left( \frac{\partial \{\phi_i\}^{Tr}}{\partial p} [K]_j \{\phi_i\} + \{\phi_i\}^{Tr} \frac{\partial [K]_j}{\partial p} \{\phi_i\} + \{\phi_i\}^{Tr} [K]_j \frac{\partial \{\phi_i\}}{\partial p} \right). \quad (26)$$

Because

$$\left[ \frac{\partial \{\phi_i\}^{Tr}}{\partial p} [MK]_j \{\phi_i\} \right]^{Tr} = \{\phi_i\}^{Tr} [K]_j \frac{\partial \{\phi_i\}}{\partial p}, \quad (27)$$

Noting that  $\left[ \frac{\partial \{\phi_i\}^{Tr}}{\partial p} [MK]_j \{\phi_i\} \right]$  is a scalar and its transpose is equal to its same value, it can be written as:

$$\frac{\partial MSEN_{ij}}{\partial p} = \{\phi_i\}^{Tr} [K]_j \frac{\partial \{\phi_i\}}{\partial p} + \frac{1}{2} \{\phi_i\}^{Tr} \frac{\partial [K]_j}{\partial p} \{\phi_i\}. \quad (28)$$

In which can be further written as:

$$\frac{\partial MSEN_{ij}}{\partial p} = \left[ \{\phi_i\}^{Tr} [K]_j \quad 0 \right] \left\{ \begin{matrix} \frac{\partial \{\phi_i\}}{\partial p} \\ \frac{\partial \omega_i}{\partial p} \end{matrix} \right\} + \frac{1}{2} \{\phi_i\}^{Tr} \frac{\partial [K]_j}{\partial p} \{\phi_i\}. \quad (29)$$

Similar to MKE<sub>n</sub> sensitivity derivation, the expression of eigenvalue and eigenvector sensitivity [20,21] can be used by inserting Equation (9) into Equation (28) as:

$$\frac{\partial MSEN_{ij}}{\partial p} = \{\phi_i\}^{Tr} \left[ [K]_j \quad 0 \right] [K_{U/D}]^{-1} [F_p] \{\phi_i\} + \frac{1}{2} \{\phi_i\}^{Tr} \frac{\partial [K]_j}{\partial p} \{\phi_i\}. \quad (30)$$

For simplicity, and similar to Equation (18), after considering the Young’s modulus change, in addition to neglecting the mass change, by using the damage parameter  $\alpha$ , Equation (30) is rewritten as:

$$\Delta MSEN_{ij} = \sum_{j=1}^n \alpha_j \{\phi_i\}^{Tr} [K^*] \{\phi_i\}, \quad (31)$$

where

$$[K^*] = \left[ [K]_j \quad 0 \right] [K_{U/D}]^{-1} [F_p] + \frac{1}{2} [K]_k. \quad (32)$$

Finally, by using Equation (25), the MSEN<sub>R</sub> sensitivity matrix  $[K^*]_i$  can be obtained by:

$$[K^*]_k = \frac{1}{\frac{1}{2} \{\phi_i\}^{Tr} [M]_j \{\phi_i\}} \left[ \left[ [K]_j \quad 0 \right] [K_{U/D}]^{-1} [F_p] + \frac{1}{2} [K]_k \right]. \quad (33)$$

Hence, Equation (17) can be simplified as:

$$[K^*] \{\alpha\} = \{\Delta R\}, \quad (34)$$

where

$$\begin{aligned} \Delta R_{ij} &= MSEN_{R_{ij}}, \text{ and} \\ K^*_{kij} &= \sum_{j=1}^n \alpha_j \frac{1}{\frac{1}{2} \{\phi_i\}^{Tr} [M]_j \{\phi_i\}} \left[ \left[ [K]_j \quad 0 \right] [K_{U/D}]^{-1} [F_p] + \frac{1}{2} [K]_k \right]. \end{aligned} \quad (35)$$

In the abovementioned description, the MREN<sub>R</sub> sensitivity of the  $j$ th element to specific change in  $k$ th member’s Young’s modulus of elasticity for the  $i$ th mode of vibration has been obtained. Additionally,  $\Delta R_{ij}$  is the MKE<sub>nR</sub> in the  $j$ th element for the  $i$ th mode of vibration. This proves the concept of damage identification using Equation (25). For further information, references [20,21] can be referred to.

### 2.3. Formulation of the Objective Function

The aforementioned deterministic mathematical approach that studies the sensitivity of modal features is vulnerable to incomplete data and noisy measurements, where any simple variation of modal parameters might lead to wrong identification. Therefore, a stochastic optimization method should be employed. Moreover, it is well-known that the structural damage identification problem is an ill-posed problem with a damage parameters region that may have multiple local optima. In this case, the traditional optimizers could be stuck in the local minima, which may deliver wrong damage identification results. Hence, it is essential to develop robust and powerful objective functions and algorithms, which could tackle the complex damage identification problem. Therefore, the use of more than one modal property contributes to improve the overall damage identification, where each property helps to discover more underlying damage information. Thus, the MSEn subobjective can be first developed based on Equations (23), (25), and (27) as:

$$F_1 = \min \left( \sum_{i=1}^N \frac{MSEn_i^D - MSEn_i}{MSEn_i} \right). \tag{36}$$

Secondly, the global  $MKE_n$  of the intact structure and the  $MKE_n^D$  of the damaged structure can be derived using the modal frequencies, mode shapes, and global mass matrix of the structure, and, based on Equations (4)–(6), the  $MKE_n$  sub-objective function can be written as:

$$F_2 = \min \left( \sum_{i=1}^N \frac{MKE_n_i^D - MKE_n_i}{MKE_n_i} \right). \tag{37}$$

Using the abovementioned damage indicator, the effect of large values of modal frequencies related to higher modes of vibration can be reduced, which makes the damage identification process faster.

In order to further improve damage deductibility when dealing with incomplete data and noisy conditions, the effect of mode shapes can be separated from the global mass and stiffness matrices. Therefore, another sub-objective, which takes advantage of the modal assurance criterion (MAC) of the mode shapes, can be written as:

$$F_3 = \min(1 - \text{mean}(\text{diag}(\text{MAC}))), \tag{38}$$

where,  $\text{diag}$  represents the diagonal elements of MAC matrix that measures the correlation between the analytical and experimental mode shapes; the MAC matrix can be written as:

$$MAC_i = \frac{|\phi_i^{DTr} \cdot \phi_i|^2}{|\phi_i^T \cdot \phi_i| |\phi_i^{DTr} \cdot \phi_i^D|}. \tag{39}$$

The MAC matrix [5] is composed of diagonal and off-diagonal elements. When measuring the correlation between two mode shapes, two correlated mode shapes should result in a MAC matrix having diagonal elements of 1, and off-diagonal elements of less than 0.1 (typically zeros). This feature is used in this sub-objective to update the FE model based on minimizing the difference between the value of one and the mean diagonal elements of the MAC matrix. When the difference is zero, there is a complete correlation between the two mode shapes; i.e., the FE model matches the current condition of the structure.

Based on Equations (36)–(38), the overall objective function of the considered optimization problem can be written as:

$$\begin{aligned} \min F = & \min \left( \sum_{i=1}^N \left( \frac{MSEn_i^D - MSEn_i}{MSEn_i} \right) + \sum_{i=1}^N \left( \frac{MKE_n_i^D - MKE_n_i}{MKE_n_i} \right) \right. \\ & \left. + (1 - \text{mean}(\text{diag}(\text{MAC}))) \right). \end{aligned} \tag{40}$$

As observed in the literature [6–32], most simulated damage scenarios are modeled as a reduction of stiffness. The reduction of stiffness can explain most commonly occurring structural damage types, such as corrosion, cracks, defects, erosion, structural element links, bolt loosening, etc. Usually, mass-related structural damage is not studied as it is mostly associated with loss of material or structural elements, which can be easily observed without a damage identification algorithm. Furthermore, as we start with the stiffness and mass matrices of the intact structure, we do not have the current condition of damaged structure matrices. Any change in stiffness will change all the modal parameters and the system matrices. Therefore, the reduction of stiffness has been used by most researchers to simulate structural damage.

The existing structural damage is often represented by a reduction in Young's modulus of elasticity, which is linearly linked to the stiffness of the structure. This might not correspond to all categories of damage, but can be referred to most common structure degradation, namely cracks, loosening of structural links, environmental corrosion, etc. Therefore, for computational purposes, the damage can be simulated as stiffness reduction or a reduction in modulus of elasticity at any element, and can be written as:

$$\Delta E_j = E_j - \alpha_j E_j, \quad (41)$$

where  $\Delta E_j$  is the damage severity and  $E_j$  is the modulus of elasticity of the intact structure;  $\alpha_j$  is the damage factor that represents the reduction in  $E_j$  for each damaged element, which is directly used as the decision parameters of the inverse problem of structural damage identification. Here, if  $\alpha_j = 1$ , there is no damage in the selected element; whereas, if  $\alpha_j = 0$ , there is a complete absence of stiffness, i.e., full damage.

### 3. The Theory of the Proposed OL-UPSGBO Algorithm

#### 3.1. Oppositional-Based Learning (OL)

When solving complex optimization problems which hide multimodality features or include several local optima, many metaheuristics tend to have slower convergence behavior or be stuck in local search areas. Recently, the OL framework has been used for overcoming the aforementioned difficulties and boosting the speed of convergence towards the optimal region. The main idea behind the OL is to compare the initial guess solution to its oppositional solution [54,55]. For one solution in the single-dimension space, the OL calculates the opposite solution using a random probability, and chooses the superior candidate solution between the initial and opposite agents, as in Figure 1. As a result, the convergence speed of the metaheuristic can be enhanced and variability in the population can be highly improved. This search enhancement can be applied both in the initialization stage and later in the main loop of the metaheuristic, or in both stages. The overall mathematical equation of OL strategy can be written as follows:

$$X_{ij}(t+1) = \begin{cases} \Delta_j + \text{rand}() \times (\Delta_j - X_{ij}(t)), & \text{if } (X_{ij}(t) < \Delta_j), \\ \Delta_j - \text{rand}() \times (X_{ij}(t) - \Delta_j), & \text{if } (X_{ij}(t) \geq \Delta_j), \end{cases} \quad (42)$$

and

$$\Delta_j = (X_j^L + X_j^U) / 2, \quad (43)$$

where  $X_{ij}(t+1)$  is the oppositional solution corresponding to  $j$ th dimension of the  $i$ th solution in the  $t$ th iteration;  $X_j^L$  and  $X_j^U$  are the lower and upper bounds;  $\Delta_j$  is the center of the distance between the upper and lower bounds of the  $j$ th dimension. The variable  $\text{rand}()$  is a uniform random number.

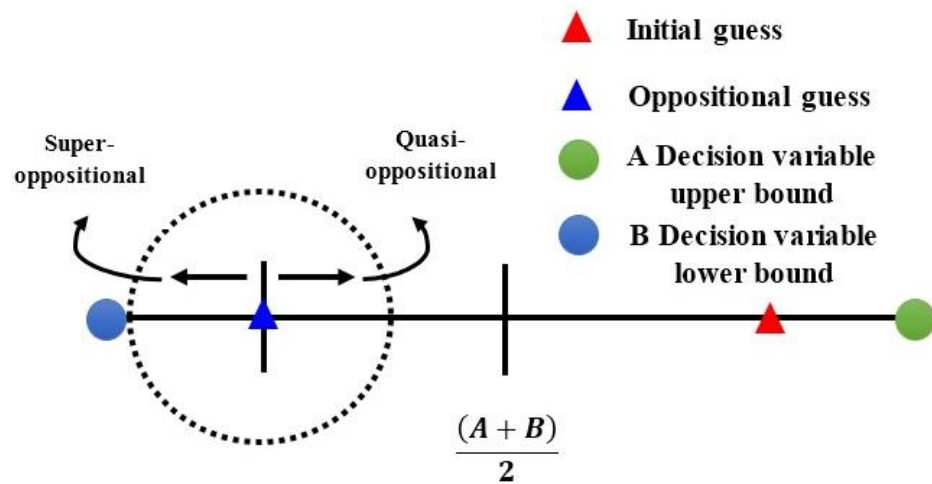


Figure 1. The OL framework.

### 3.2. The UPSO

The UPSO was originally proposed by Parsopoulos and Vrahatis [36] in order to provide a balance between exploration and exploitation schemes; specifically, to balance the cognitive and social paradigms of the original constriction PSO. It is well-known that the PSO is composed of two main schemes, namely the global neighborhood-based scheme, in which the whole swarm is guided by the swarm superior particle, and the local neighborhood-based scheme, which relies on the use of smaller swarms guided by the local superior particle. According to the constriction scheme developed by Clerc and Kennedy [56], the particle  $X$  updates its position using the following equations as:

$$\begin{aligned} V_i(t+1) &= \Omega[V_i(t) + c_1r_1(P_i(t) - X_i(t)) + c_2r_2(P_{s_i}(t) - X_i(t))], \\ X_i(t+1) &= X_i(t) + V_{i+1}(t+1), \end{aligned} \tag{44}$$

where  $V_i(t)$  is the  $i$ th velocity at  $t$ th iteration;  $\Omega$  is the constriction coefficient;  $c$  coefficients are constants which indicate the cognitive and social factors;  $r$  variables are two random numbers  $\in [0, 1]$ ;  $P_G$  is the global superior particle;  $P_{s_i}$  is the local superior particle performance;  $\Omega$ ,  $c_1$ , and  $c_2$  can be determined from [36].

The UPSO was originally introduced to find a balance between the global and local schemes, or the exploration and exploitation of the original behavior of PSO. Let  $G_i(t+1)$  and  $L_i(t+1)$  be the particle  $X_i$  velocity related to global and local schemes, respectively, it can then be written as:

$$\begin{aligned} G_i(t+1) &= \Omega[V_i(t) + c_1r_1(P_i(t) - X_i(t)) + c_2r_2(P_s(t) - X_i(t))], \\ L_i(t+1) &= \Omega[V_i(t) + c_1r'1(P_i(t) - X_i(t)) + c_2r'2(P_{s_i}(t) - X_i(t))], \end{aligned} \tag{45}$$

where  $s$  is the index of the superior particle of the whole swarm (global variant); and  $s_i$  is the index of the superior particle in the neighborhood of  $X_i$  (local variant). The UPSO mathematical framework is defined as:

$$\begin{aligned} U_i(t+1) &= (1 - \mu)L_i(t+1) + \mu G_i(t+1), \\ X_i(t+1) &= X_i(t) + U_i(t+1), \end{aligned} \tag{46}$$

where  $\mu$  is a constant factor number  $\in [0, 1]$ , called the unification factor, that balances both local and global schemes of UPSO. When  $\mu = 1$ , the UPSO behaves same as the original global PSO, whereas  $\mu = 0$ , the UPSO behaves same as the original local PSO. The various values of the unification factor correspond to various combinations of exploration-exploitation paradigms of UPSO. Nevertheless, it was recommended by Tsai [57] that

$\mu = 0.5$ , and can provide the best balance in UPSO behavior and will be considered in this study.

### 3.3. The GBO Algorithm

The GBO algorithm [53] was originally proposed to modify the Newtonian principle of gradient-based optimization and integrate it with the theory of population-based optimization to form a power algorithm able to solve complex problems. The GBO has three stages, namely the initialization stage, the gradient search rule (GSR) stage, and the local escaping stage. The GBO stages are summarized as follows.

#### 3.3.1. The Initialization Stage

Similar to other ECs, the GBO needs to randomly create a group of initial candidate solutions. The initial set of solution vectors has  $N \times D$  dimensions, where  $N$  is the number of candidate vectors and  $D$  is the dimension of the problem. The initialization can be performed using the following equation as:

$$v_n = v_{min} + rand(0, 1) \times (v_{max} - v_{min}), \tag{47}$$

where  $v_{min}$  and  $v_{max}$  are the bound constraints of the decision variable  $v$ , and  $rand(0, 1)$  is a randomly generated number  $\in [0, 1]$ .

#### 3.3.2. The GSR Stage

After the initialization of the population, the search for an optimal solution begins by maintaining and balancing the exploration and exploitation around the optimal solution. For this purpose, a stochastic parameter, called  $\rho_1$ , can be calculated as:

$$\rho_1 = \alpha \times (2 \times rand - 1), \tag{48}$$

where the operator  $\alpha$  can be calculated as:

$$\alpha = \left| \beta \times \sin\left(\frac{3\pi}{2} + \sin\left(\beta \times \frac{3\pi}{2}\right)\right) \right|, \tag{49}$$

and the operator  $\beta$  can be realized as:

$$\beta = \beta_{min} \left( 1 + (\beta_{max} - 1) \left( 1 - \left( \frac{i}{i_{max}} \right)^3 \right)^2 \right), \tag{50}$$

where  $[\beta_{min}, \beta_{max}] = [0.2, 1.2]$ ,  $i$  is the current generation number and  $i_{max}$  is the total number of generations. The variations of  $\alpha$  in a decreasing and increasing way during the algorithm's execution contribute to changing the value of  $\rho_1$  in a sinusoidal fashion, which gives better variability of exploration and exploitation in the search space. Hence, the GSR can be calculated as follows:

$$GSR = randn \times \rho_1 \times \frac{2 \times \Delta v \times v_n}{(v_{worst} - v_{best} + \epsilon)}, \tag{51}$$

where  $\Delta v$  is defined based on the variation between  $v_{best}$  and  $v_{r1}^i$  that is a randomly selected solution vector iteration.  $i$ ,  $v_{worst}$ , and  $v_{best}$  are the current best and worst solution vectors,  $v_n$  is the current solution vector, and  $\epsilon$  is a constant.

In order to ensure that the  $\Delta v$  is not fixed during the running of the algorithm and to boost the exploration, another parameter  $\delta$  is calculated, as in Equation (54).

$$\Delta v = rand(: N) \times |step|, \tag{52}$$

where

$$step = \frac{(v_{best} - v_{r1}^t) + \delta}{2}, \tag{53}$$

and

$$\delta = 2 \times rand \times \left( \left| \frac{v_{r1}^t + v_{r2}^t + v_{r3}^t + v_{r4}^t}{4} - v_n^t \right| \right), \tag{54}$$

where *rand* is a random vector with *N* dimensions, parameters *r*<sub>1</sub>, *r*<sub>2</sub>, *r*<sub>3</sub>, and *r*<sub>4</sub> are four different randomly selected integers ∈ [1, *N*], and *step* is the step size.

Another term is added to further promote the abilities of GBO and provide better exploration, which is the direction movement (*DM*); this takes advantage of the *v*<sub>best</sub> and moves the current position *v*<sub>*n*</sub> towards (*v*<sub>best</sub> - *v*<sub>*n*</sub>) and can be defined as:

$$MD = randn \times \rho_2 \times (v_{best} - v_n), \tag{55}$$

where *randn* is a random number ∈ [0, 1], and  $\rho_2$  a stochastic parameter aids to give every solution vector unequal step, the parameter  $\rho_2$  is another important stochastic parameter similar to  $\rho_1$  as two leading stochastic influencers of GBO. The parameter  $\eta$  can be expressed as:

$$\rho_2 = \alpha \times (2 \times rand - 1), \tag{56}$$

Finally, based on the *GSR* and *DM*, Equations (51) and (55) are used to update the current vector (*v*<sub>*n*</sub><sup>*i*</sup>) as follows:

$$v1_n^i = v_n^i - GSR + DM, \tag{57}$$

where *v1*<sub>*n*</sub><sup>*i*</sup> is the new solution vector after updating *v*<sub>*n*</sub><sup>*i*</sup>. Moreover, Equation (30) can be further reformed as follows:

$$v1_n^i = v_n^i - randn \times \rho_1 \times \frac{2 \times \Delta v \times v_n^i}{(up_n^i - uq_n^i + \epsilon)} + randn \times \rho_2 \times (v_{best} - v_n^i) \tag{58}$$

where *up*<sub>*n*</sub><sup>*i*</sup> and *uq*<sub>*n*</sub><sup>*i*</sup> are equal to *u*<sub>*n*</sub> +  $\Delta v$  and *u*<sub>*n*</sub> -  $\Delta v$ , *u*<sub>*n*</sub> is the average vector between the current vector *v*<sub>*n*</sub> and *z*<sub>*n*+1</sub> vector, which is calculated as:

$$z_{n+1} = v_n - randn \times \rho_1 \times \frac{2 \times \Delta v \times v_n}{(v_{worst} - v_{best} + \epsilon)}, \tag{59}$$

Another stochastic position updating *v2*<sub>*n*</sub><sup>*i*</sup> can be adopted by replacing *v*<sub>best</sub> and *v*<sub>*n*</sub> in Equation (58) with two randomly selected vectors, *v*<sub>*r1*</sub><sup>*i*</sup> and *v*<sub>*r2*</sub><sup>*i*</sup>; the new vector can be calculated as follows:

$$v2_n^i = v_n^i - randn \times \rho_1 \times \frac{2 \times \Delta v \times v_n^i}{(up_n^i - uq_n^i + \epsilon)} + randn \times \rho_2 \times (v_{r1}^i - v_{r2}^i). \tag{60}$$

The main contribution of Equation (58) is to govern the exploration procedure of GBO; whereas, the primary mechanism of Equation (60) serves to perform the exploitation framework. Therefore, based on the vectors *v1*<sub>*n*</sub> and *v2*<sub>*n*</sub>, the leading mathematical term of GBO that updates the position of *v*<sub>*n*</sub><sup>*i*</sup> can be expressed as:

$$v_n^{i+1} = r_a \times (r_b \times v1_n^i + (1 - r_b) \times v2_n^i) + (1 - r_a) \times v3_n^i, \tag{61}$$

where

$$v3_n^i = v_n - \rho_1 \times (v2_n^i - v1_n^i), \tag{62}$$

and *r*<sub>*a*</sub> and *r*<sub>*b*</sub> are two random variables ∈ [0, 1].

### 3.3.3. The Local Escaping Stage

To improve the main search mechanism of GBO and adapt its behavior to solve more complex optimization problems, the local escaping paradigm (LEP) was introduced in [53]. The LEP aims to guide the current solution vector to escape from the local search area and prevent the GBO from giving local optimum solutions. The LEP adopts two main equations, as follows:

$$v_{LEP} = \begin{cases} \begin{cases} v_n^{i+1} + \sigma_1 \times (\gamma_1 \times v_{best} - \gamma_2 \times v_r) \\ + \sigma_2 \times \rho_1 \times \gamma_3 \times (v2_n^i - v1_n^i) / 2 \\ + \sigma_2 \times \rho_1 \gamma_2 \times (v_{r1}^i - v_{r2}^i) / 2, \end{cases} & \text{if } rand < 0.5, \\ \begin{cases} v_{best} + \sigma_1 \times (\gamma_1 \times v_{best} - \gamma_2 \times v_r) \\ + \sigma_2 \times \rho_1 \times \gamma_3 \times (v2_n^i - v1_n^i) / 2 \\ + \sigma_2 \times \rho_1 \times \gamma_2 \times (v_{r1}^i - v_{r2}^i) / 2, \end{cases} & \text{otherwise,} \end{cases} \quad (63)$$

where  $\sigma_1$  and  $\sigma_2$  are Gaussian uniform distribution random number  $\in [-1, 1]$ ,  $v_r$  is a randomly selected solution vector, and  $\gamma_1, \gamma_2,$  and  $\gamma_3$  are random numbers that can be calculated as:

$$\begin{bmatrix} \gamma_1 \\ \gamma_2 \\ \gamma_3 \end{bmatrix} = \begin{cases} \begin{cases} 2 \times rand & \text{if } u_1 < 0.5 \\ 1 & \text{else,} \end{cases} \\ \begin{cases} rand & \text{if } u_1 < 0.5 \\ 1 & \text{else,} \end{cases} \\ \begin{cases} rand & \text{if } u_1 < 0.5 \\ 1 & \text{else,} \end{cases} \end{cases} \quad (64)$$

where  $rand$  is a random variable  $\in [0 - 1]$ , and  $u_1$  is a probability rate.

To generate the random solution vector  $v_r$  in Equation (63), the following expression is employed:

$$v_r = \begin{cases} v_{min} + r \times (v_{max} - v_{min}) & \text{if } rand < 0.5, \\ v_{ra} & \text{else,} \end{cases} \quad (65)$$

where  $v_{ra}$  is a randomly chosen vector from the population, and  $rand$  is a probability rate. The GBO flowchart is shown in Figure 2 and the overall mathematical visualization of GBO can be observed in Figure 3.

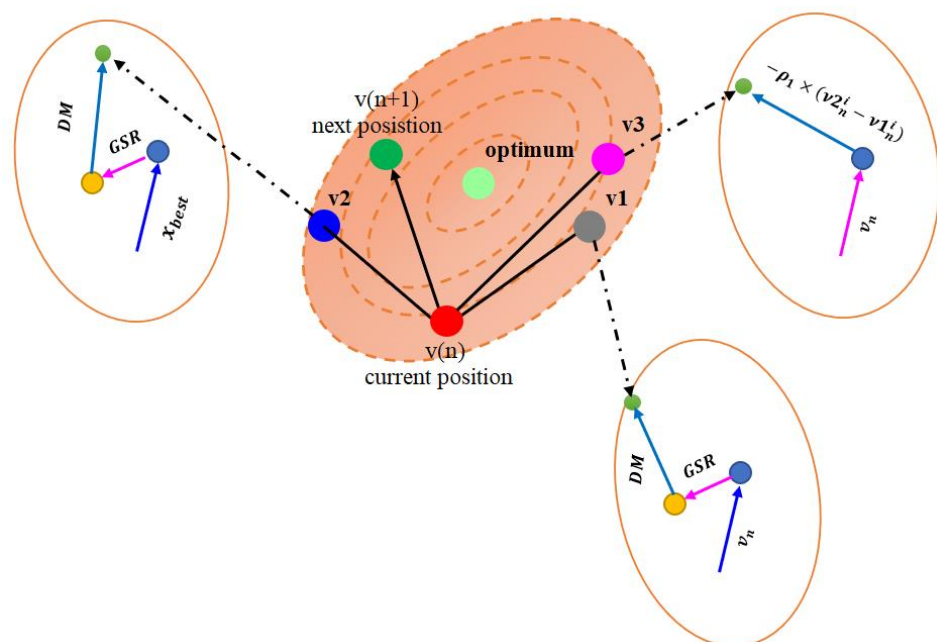
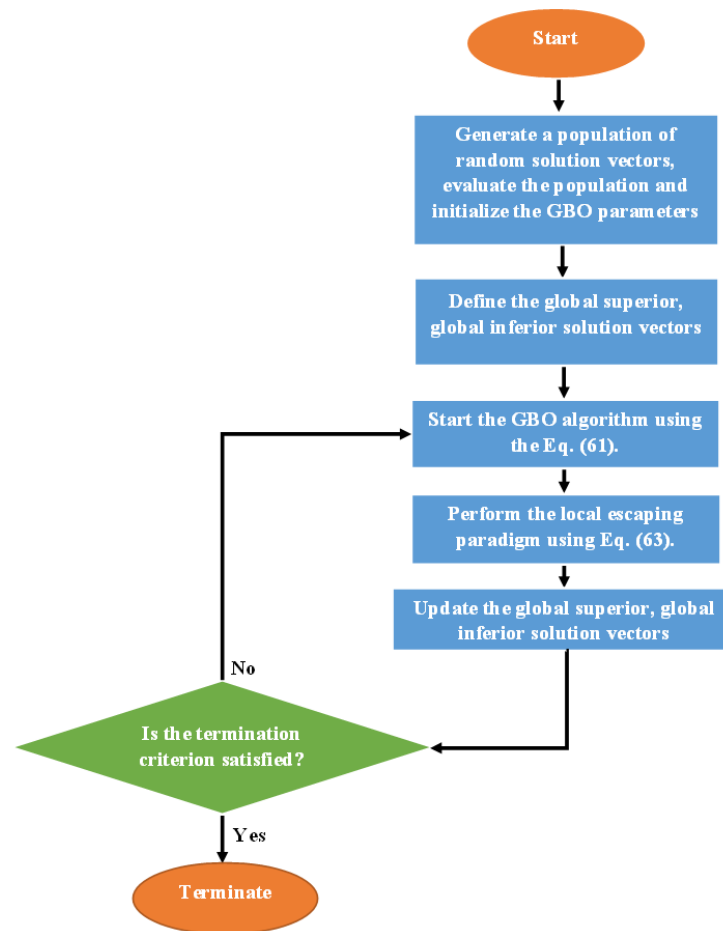


Figure 2. The GBO algorithm.



**Figure 3.** The GBO algorithm flowchart.

### 3.4. The Proposed OL-UPSGBO Algorithm

In order to provide an enhanced optimization algorithm that is able to tackle the inverse analysis of structural damage problems, the OL-UPSGBO is proposed. The new OL-UPSGBO puts to use the aforementioned search paradigms, which serve to boost the search performance and overcome the complex features of the inverse problem, in which there is no direct link between the search agents and the objective function. Within the framework of OL-UPSGBO, the algorithm takes advantage of the OL procedure in both the initialization of the population of the search agents, as well as inside the iterative phase. The main iterative evolutionary procedure first exploits the UPSO algorithm procedure to select the global, local, and best performed search agents and improve them in each iteration. Later, the GBO utilizes the improved elite search agents to perform the main optimization task. Thereafter, the OL improves the convergence of the algorithm within the iterative phase. The overall schematic diagram of the developed OL-UPSGBO algorithm can be observed in Figure 4.

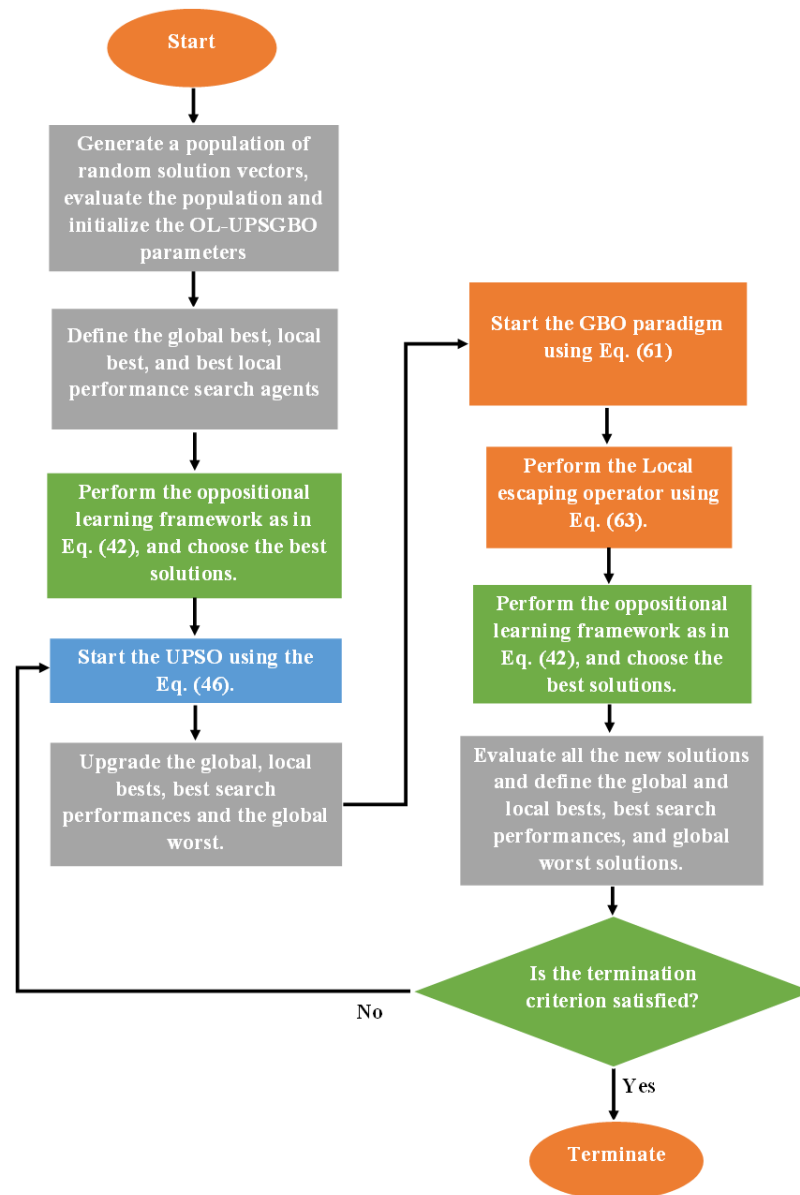


**Figure 4.** The flowchart of the proposed OL-UPSGBO algorithm.

### 3.5. Benchmarking of the OL-UPSGBO Algorithm

To benchmark the performance of the proposed OL-UPSGBO algorithm, the IEEE CEC 2017 test suite is utilized [58,59]. The CEC 2017 benchmark objective function set is one of the most complex bound constraint benchmark functions. It contains 30 objective functions in which functions  $[F_1 - F_2]$  are unimodal,  $[F_3 - F_9]$  are multimodal,  $[F_{11} - F_{20}]$  are hybrid, and  $[F_{21} - F_{30}]$  are composite functions. The essential functions on which CEC 2017 test suite is built are shown in Table 1, as well as in [58,59].

**Table 1.** The CEC 2017 test suite [58,59].

Function Type	No.	Function	Optimum
Unimodal	$F_1$	Shifted and Rotated Bent Cigar Function	100
	$F_2$	NA	NA
	$F_3$	Shifted and Rotated Zakharov Function	300
Multimodal	$F_4$	Shifted and Rotated Rosenbrock's Function	400
	$F_5$	Shifted and Rotated Rastrigin's Function	500
	$F_6$	Shifted and Rotated Expanded Scaffer's $f_6$ Function	600
	$F_7$	Shifted and Rotated Lunacek Bi_Rastrigin Function	700
	$F_8$	Shifted and Rotated Non-Continuous Rastrigin's Function	800
	$F_9$	Shifted and Rotated Levy Function	900
	$F_{10}$	Shifted and Rotated Schwefel's Function	1000
	Hybrid	$F_{11}$	Hybrid Function 1 (N = 3)
$F_{12}$		Hybrid Function 2 (N = 3)	1200
$F_{13}$		Hybrid Function 3 (N = 3)	1300
$F_{14}$		Hybrid Function 4 (N = 4)	1400
$F_{15}$		Hybrid Function 5 (N = 4)	1500
$F_{16}$		Hybrid Function 6 (N = 4)	1600
$F_{17}$		Hybrid Function 6 (N = 5)	1700
$F_{18}$		Hybrid Function 6 (N = 5)	1800
$F_{19}$		Hybrid Function 6 (N = 5)	1900
$F_{20}$		Hybrid Function 6 (N = 6)	2000
Composite	$F_{21}$	Composition Function 1 (N = 3)	2100
	$F_{22}$	Composition Function 2 (N = 3)	2200
	$F_{23}$	Composition Function 3 (N = 4)	2300
	$F_{24}$	Composition Function 4 (N = 4)	2400
	$F_{25}$	Composition Function 5 (N = 5)	2500
	$F_{26}$	Composition Function 6 (N = 5)	2600
	$F_{27}$	Composition Function 7 (N = 6)	2700
	$F_{28}$	Composition Function 8 (N = 6)	2800
	$F_{29}$	Composition Function 9 (N = 3)	2900
	$F_{30}$	Composition Function 10 (N = 3)	3000

Bearing in mind the explicit complexity of the CEC 2017 test suite and the nature of the hybrid and composite functions, the OL-UPSGBO is tested using a dimension of 30 search agents. According to the CEC recommendations, the overall number of evaluations is set at 200,000 evaluations. Each algorithm execution is conducted 20 times for each function. Using this framework, the proposed OL-UPSGBO is compared to five other MHS: the original the Gray Wolf Optimizer (GWO) [60], the Whale Optimization Algorithm (WOA) [61], the Multi-verse Optimizer (MVO) [62], the Sine Cosine Algorithm (SCA) [63], the GBO [53], the Arithmetic Optimization Algorithm (AOA) [64], the Equilibrium Optimizer (EO) [65], and the Aquilla Optimizer (AO) [66]. The stochastic parameters of each MH are set as the original recommended settings suggested by each paper, as in Table 2. The parametric statistical comparison is made using the mean, best, worst, and standard deviation (STD). All the outcomes of executing the algorithm mentioned above are presented in Table 3 for the unimodal and multi-modal, hybrid, and composite functions, respectively.

Moreover, the Friedman test and Wilcoxon test were conducted as two non-parametric statistical tests. The average ranking and total ranking based on the Friedman test can be observed in the last two rows of Table 3, which show that the proposed OLUPSGBO has the best rank among the tested algorithms. Furthermore, to further graphically illustrate the Friedman test ranks, the total ranks can be seen in Figure 5. The Wilcoxon test was also conducted and *p*-value results of the test can be tabulated in Table 4. It is clear that the OLUPSUBO algorithm is statistically significant to other algorithms corresponding to most studied functions with a *p*-value <0.05. Nevertheless, it is common to have statistical similarities between the algorithms for fewer cases. The overall results demonstrate that the proposed OL-UPSGBO algorithm has great performance when compared with the studied algorithms and the component algorithms for higher dimensions using the CEC 2017 test suite. In addition, the convergence curves of some tested algorithms can be observed in Figure 6. By studying the test results, it is evident that the OL-UPSGBO algorithm is statistically significant for most of CEC 2017 test functions; hence, the proposed OL-UPSGBO algorithm can be highly implemented for solving modern complex optimization problems and practical engineering optimization problems, such as the inverse analysis of structural damage problem.

**Table 2.** Stochastic parameter settings for the compared algorithms.

Algorithm	Parameters
GWO	Default stochastic parameter descending from 2 to 0.
WOA	Default stochastic parameter one descending from 2 to 0.
SCA	Default stochastic parameter two descending from 2 to 0.
MVO	Traveling distance rate (default) Wormhole existence probability (default)
AOA	Default stochastic parameters: MOP_Max = 1; MOP_Min = 0.2; Alpha = 5; Mu = 0.499;
EO	Default stochastic parameters: a1 = 5; a2 = 1; GP = 0.5;
AO	Default stochastic parameters: alpha = 0.1; delta = 0.1;
OL-UPSGBO	$\beta_{min} = 0.2$ (default) $\beta_{max} = 1.2$ (default) $\xi = 0.5$ (default)

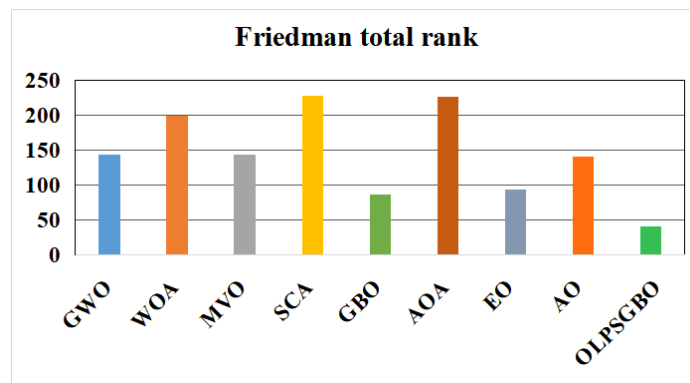


**Figure 5.** The total rank results of the Friedman test.

**Table 3.** The benchmarking of the OL-UPSGBO algorithm for the CEC 2017.

Function	Property	GWO	WOA	MVO	SCA	GBO	AOA	EO	AO	OLPSGBO
$F_1$	Ave	$1.1 \times 10^9$	$2.6 \times 10^6$	$3.7 \times 10^8$	$1.6 \times 10^{10}$	$1.9 \times 10^3$	$2.0 \times 10^8$	$5.6 \times 10^3$	$3.0 \times 10^2$	$1.5 \times 10^2$
	Min	$5.5 \times 10^8$	$7.2 \times 10^5$	$2.8 \times 10^8$	$1.0 \times 10^{10}$	$3.2 \times 10^2$	$9.4 \times 10^3$	$1.2 \times 10^2$	$1.1 \times 10^2$	$1.0 \times 10^2$
	Max	$2.7 \times 10^9$	$5.3 \times 10^6$	$4.2 \times 10^8$	$2.1 \times 10^{10}$	$5.1 \times 10^3$	$8.2 \times 10^8$	$1.7 \times 10^4$	$9.2 \times 10^2$	$2.9 \times 10^2$
	STD	$6.5 \times 10^8$	$1.2 \times 10^6$	$4.5 \times 10^7$	$2.8 \times 10^9$	$1.9 \times 10^3$	$3.0 \times 10^8$	$5.3 \times 10^3$	$2.5 \times 10^2$	$7.4 \times 10^1$
	Rank	8	5	7	9	3	6	4	2	1
$F_2$	NA	NA	NA	NA	NA	NA	NA	NA	NA	NA
$F_3$	Ave	$2.9 \times 10^4$	$2.0 \times 10^5$	$1.8 \times 10^3$	$4.5 \times 10^4$	$3.0 \times 10^2$	$7.8 \times 10^4$	$7.3 \times 10^2$	$3.0 \times 10^4$	$3.0 \times 10^2$
	Min	$8.3 \times 10^3$	$9.9 \times 10^4$	$1.6 \times 10^3$	$4.0 \times 10^4$	$3.0 \times 10^2$	$6.0 \times 10^4$	$4.0 \times 10^2$	$2.1 \times 10^4$	$3.0 \times 10^2$
	Max	$3.9 \times 10^4$	$3.5 \times 10^5$	$2.0 \times 10^3$	$5.6 \times 10^4$	$3.0 \times 10^2$	$8.8 \times 10^4$	$1.4 \times 10^3$	$3.5 \times 10^4$	$3.0 \times 10^2$
	STD	$9.0 \times 10^3$	$7.6 \times 10^4$	$1.4 \times 10^2$	$5.3 \times 10^4$	$2.3 \times 10^{-2}$	$9.5 \times 10^3$	$3.3 \times 10^2$	$4.9 \times 10^3$	$1.3 \times 10^{-3}$
	Rank	8	5	7	9	3	6	4	2	1
$F_4$	Ave	$5.8 \times 10^2$	$5.6 \times 10^2$	$5.2 \times 10^2$	$1.6 \times 10^3$	$4.5 \times 10^2$	$1.0 \times 10^4$	$5.0 \times 10^2$	$5.5 \times 10^2$	$4.0 \times 10^2$
	Min	$5.4 \times 10^2$	$4.8 \times 10^2$	$5.0 \times 10^2$	$1.2 \times 10^3$	$4.0 \times 10^2$	$5.6 \times 10^3$	$4.7 \times 10^2$	$5.2 \times 10^2$	$4.0 \times 10^2$
	Max	$6.3 \times 10^2$	$6.5 \times 10^2$	$5.3 \times 10^2$	$2.3 \times 10^3$	$4.8 \times 10^2$	$1.3 \times 10^4$	$5.2 \times 10^2$	$6.1 \times 10^2$	$4.0 \times 10^2$
	STD	$3.4 \times 10^1$	$4.6 \times 10^1$	$1.2 \times 10^1$	$3.5 \times 10^2$	$3.1 \times 10^1$	$2.6 \times 10^3$	$1.6 \times 10^1$	$2.9 \times 10^1$	$2.1 \times 10^2$
	Rank	8	5	7	9	3	6	4	2	1
$F_5$	Ave	$5.7 \times 10^2$	$7.9 \times 10^2$	$7.0 \times 10^2$	$8.0 \times 10^2$	$6.7 \times 10^2$	$8.2 \times 10^2$	$5.6 \times 10^2$	$6.7 \times 10^2$	$6.3 \times 10^2$
	Min	$5.6 \times 10^2$	$7.1 \times 10^2$	$6.7 \times 10^2$	$7.7 \times 10^2$	$6.2 \times 10^2$	$7.5 \times 10^2$	$5.3 \times 10^2$	$6.4 \times 10^2$	$5.8 \times 10^2$
	Max	$6.0 \times 10^2$	$9.5 \times 10^2$	$7.3 \times 10^2$	$8.2 \times 10^2$	$7.1 \times 10^2$	$8.6 \times 10^2$	$6.0 \times 10^2$	$7.0 \times 10^2$	$6.6 \times 10^2$
	STD	$1.4 \times 10^1$	$7.1 \times 10^1$	$2.1 \times 10^1$	$1.7 \times 10^1$	$2.4 \times 10^1$	$3.4 \times 10^1$	$2.0 \times 10^1$	$2.0 \times 10^1$	$2.9 \times 10^1$
	Rank	2	7	6	8	5	9	1	4	3
$F_6$	Ave	$6.1 \times 10^2$	$6.7 \times 10^2$	$6.2 \times 10^2$	$6.6 \times 10^2$	$6.2 \times 10^2$	$6.7 \times 10^2$	$6.0 \times 10^2$	$6.5 \times 10^2$	$6.1 \times 10^2$
	Min	$6.1 \times 10^2$	$6.6 \times 10^2$	$6.1 \times 10^2$	$6.5 \times 10^2$	$6.1 \times 10^2$	$6.5 \times 10^2$	$6.0 \times 10^2$	$6.4 \times 10^2$	$6.0 \times 10^2$
	Max	$6.2 \times 10^2$	$6.8 \times 10^2$	$6.3 \times 10^2$	$6.7 \times 10^2$	$6.2 \times 10^2$	$6.7 \times 10^2$	$6.0 \times 10^2$	$6.5 \times 10^2$	$6.2 \times 10^2$
	STD	$2.0 \times 10^1$	$7.1 \times 10^1$	$7.3 \times 10^1$	$6.0 \times 10^1$	$4.9 \times 10^1$	$6.4 \times 10^1$	$8.0 \times 10^{-2}$	$5.4 \times 10^1$	$6.0 \times 10^1$
	Rank	3	9	4	7	5	8	1	6	2
$F_7$	Ave	$9.3 \times 10^2$	$1.3 \times 10^3$	$9.8 \times 10^2$	$1.1 \times 10^3$	$9.3 \times 10^2$	$1.3 \times 10^3$	$8.0 \times 10^2$	$1.0 \times 10^3$	$8.8 \times 10^2$
	Min	$9.1 \times 10^2$	$1.1 \times 10^3$	$9.4 \times 10^2$	$1.1 \times 10^3$	$8.9 \times 10^2$	$1.2 \times 10^3$	$7.6 \times 10^2$	$9.4 \times 10^2$	$8.2 \times 10^2$
	Max	$9.6 \times 10^2$	$1.5 \times 10^3$	$1.0 \times 10^2$	$1.2 \times 10^3$	$9.8 \times 10^2$	$1.4 \times 10^3$	$8.3 \times 10^2$	$1.1 \times 10^3$	$9.2 \times 10^2$
	STD	$1.6 \times 10^1$	$1.1 \times 10^2$	$2.4 \times 10^1$	$2.4 \times 10^1$	$3.3 \times 10^1$	$4.8 \times 10^1$	$2.0 \times 10^1$	$5.1 \times 10^1$	$3.0 \times 10^1$
	Rank	4	8	5	7	3	9	1	6	2
$F_8$	Ave	$9.4 \times 10^2$	$1.0 \times 10^3$	$1.0 \times 10^3$	$1.1 \times 10^3$	$9.3 \times 10^2$	$1.1 \times 10^3$	$8.7 \times 10^2$	$9.3 \times 10^2$	$9.1 \times 10^2$
	Min	$9.1 \times 10^2$	$9.6 \times 10^2$	$9.7 \times 10^2$	$1.0 \times 10^3$	$8.9 \times 10^2$	$1.0 \times 10^3$	$8.4 \times 10^2$	$8.9 \times 10^2$	$8.8 \times 10^2$
	Max	$9.6 \times 10^2$	$1.1 \times 10^3$	$1.1 \times 10^3$	$1.1 \times 10^3$	$9.8 \times 10^2$	$1.1 \times 10^3$	$9.0 \times 10^2$	$9.6 \times 10^2$	$9.3 \times 10^2$
	STD	$1.4 \times 10^1$	$6.3 \times 10^1$	$4.0 \times 10^1$	$1.6 \times 10^1$	$3.3 \times 10^1$	$3.4 \times 10^1$	$1.9 \times 10^1$	$2.3 \times 10^1$	$1.8 \times 10^1$
	Rank	5	6	7	9	4	8	1	3	2
$F_9$	Ave	$1.7 \times 10^3$	$7.5 \times 10^3$	$1.3 \times 10^3$	$5.6 \times 10^3$	$2.0 \times 10^3$	$5.8 \times 10^3$	$9.0 \times 10^2$	$5.2 \times 10^3$	$1.6 \times 10^3$
	Min	$1.2 \times 10^3$	$5.1 \times 10^3$	$1.0 \times 10^3$	$4.4 \times 10^3$	$1.4 \times 10^3$	$4.5 \times 10^3$	$9.0 \times 10^2$	$3.5 \times 10^3$	$1.2 \times 10^3$
	Max	$2.4 \times 10^3$	$1.0 \times 10^4$	$2.5 \times 10^3$	$6.5 \times 10^3$	$3.3 \times 10^3$	$7.2 \times 10^3$	$9.1 \times 10^2$	$7.1 \times 10^3$	$2.1 \times 10^3$
	STD	$3.5 \times 10^2$	$1.8 \times 10^3$	$4.7 \times 10^2$	$6.8 \times 10^2$	$6.2 \times 10^2$	$8.0 \times 10^2$	$4.5 \times 10^1$	$1.1 \times 10^3$	$3.1 \times 10^2$
	Rank	5	6	7	9	4	8	1	3	2

Table 3. Cont.

Function	Property	GWO	WOA	MVO	SCA	GBO	AOA	EO	AO	OLPSGBO
F <sub>10</sub>	Ave	5.9 × 10 <sup>3</sup>	6.4 × 10 <sup>3</sup>	7.2 × 10 <sup>3</sup>	8.2 × 10 <sup>3</sup>	5.1 × 10 <sup>3</sup>	6.8 × 10 <sup>3</sup>	4.6 × 10 <sup>3</sup>	4.9 × 10 <sup>3</sup>	4.5 × 10 <sup>3</sup>
	Min	4.7 × 10 <sup>3</sup>	5.3 × 10 <sup>3</sup>	6.6 × 10 <sup>3</sup>	7.4 × 10 <sup>3</sup>	4.5 × 10 <sup>3</sup>	6.0 × 10 <sup>3</sup>	3.3 × 10 <sup>3</sup>	4.0 × 10 <sup>3</sup>	3.8 × 10 <sup>3</sup>
	Max	6.5 × 10 <sup>3</sup>	8.4 × 10 <sup>3</sup>	8.1 × 10 <sup>3</sup>	8.7 × 10 <sup>3</sup>	7.0 × 10 <sup>3</sup>	7.7 × 10 <sup>3</sup>	5.8 × 10 <sup>3</sup>	5.7 × 10 <sup>3</sup>	5.2 × 10 <sup>3</sup>
	STD	5.4 × 10 <sup>2</sup>	1.0 × 10 <sup>3</sup>	4.8 × 10 <sup>2</sup>	4.0 × 10 <sup>2</sup>	7.5 × 10 <sup>2</sup>	5.7 × 10 <sup>2</sup>	8.6 × 10 <sup>2</sup>	5.4 × 10 <sup>2</sup>	4.1 × 10 <sup>2</sup>
	Rank	5	6	7	9	4	8	1	3	2
F <sub>11</sub>	Ave	1.5 × 10 <sup>3</sup>	1.5 × 10 <sup>3</sup>	1.4 × 10 <sup>3</sup>	2.4 × 10 <sup>3</sup>	1.2 × 10 <sup>3</sup>	4.4 × 10 <sup>3</sup>	1.4 × 10 <sup>3</sup>	1.4 × 10 <sup>3</sup>	1.2 × 10 <sup>3</sup>
	Min	1.3 × 10 <sup>3</sup>	1.3 × 10 <sup>3</sup>	1.3 × 10 <sup>3</sup>	2.0 × 10 <sup>3</sup>	1.2 × 10 <sup>3</sup>	1.8 × 10 <sup>3</sup>	1.3 × 10 <sup>3</sup>	1.3 × 10 <sup>3</sup>	1.2 × 10 <sup>3</sup>
	Max	2.1 × 10 <sup>3</sup>	1.7 × 10 <sup>3</sup>	1.5 × 10 <sup>3</sup>	2.9 × 10 <sup>3</sup>	1.3 × 10 <sup>3</sup>	8.6 × 10 <sup>3</sup>	1.4 × 10 <sup>3</sup>	1.5 × 10 <sup>3</sup>	1.2 × 10 <sup>3</sup>
	STD	2.7 × 10 <sup>2</sup>	1.5 × 10 <sup>2</sup>	4.9 × 10 <sup>1</sup>	3.3 × 10 <sup>2</sup>	2.7 × 10 <sup>1</sup>	2.3 × 10 <sup>3</sup>	6.5 × 10 <sup>1</sup>	6.3 × 10 <sup>1</sup>	1.1 × 10 <sup>1</sup>
	Rank	7	6	5	8	2	9	3	4	1
F <sub>12</sub>	Ave	9.6 × 10 <sup>7</sup>	4.1 × 10 <sup>7</sup>	4.7 × 10 <sup>7</sup>	1.5 × 10 <sup>9</sup>	2.9 × 10 <sup>4</sup>	9.2 × 10 <sup>9</sup>	7.5 × 10 <sup>5</sup>	1.5 × 10 <sup>7</sup>	2.9 × 10 <sup>4</sup>
	Min	5.5 × 10 <sup>7</sup>	9.3 × 10 <sup>6</sup>	3.4 × 10 <sup>7</sup>	7.6 × 10 <sup>8</sup>	1.3 × 10 <sup>4</sup>	4.0 × 10 <sup>9</sup>	3.0 × 10 <sup>5</sup>	3.0 × 10 <sup>6</sup>	1.3 × 10 <sup>4</sup>
	Max	1.8 × 10 <sup>8</sup>	1.4 × 10 <sup>8</sup>	7.0 × 10 <sup>7</sup>	2.2 × 10 <sup>9</sup>	4.2 × 10 <sup>4</sup>	1.2 × 10 <sup>10</sup>	2.0 × 10 <sup>6</sup>	2.6 × 10 <sup>7</sup>	4.3 × 10 <sup>4</sup>
	STD	4.1 × 10 <sup>7</sup>	3.8 × 10 <sup>7</sup>	1.2 × 10 <sup>7</sup>	5.0 × 10 <sup>8</sup>	1.0 × 10 <sup>4</sup>	2.6 × 10 <sup>9</sup>	5.1 × 10 <sup>5</sup>	6.9 × 10 <sup>6</sup>	1.1 × 10 <sup>4</sup>
	Rank	7	6	5	8	2	9	3	4	1
F <sub>13</sub>	Ave	2.5 × 10 <sup>7</sup>	1.1 × 10 <sup>5</sup>	1.7 × 10 <sup>7</sup>	6.4 × 10 <sup>8</sup>	1.0 × 10 <sup>4</sup>	9.3 × 10 <sup>7</sup>	4.3 × 10 <sup>4</sup>	3.2 × 10 <sup>5</sup>	7.6 × 10 <sup>3</sup>
	Min	1.2 × 10 <sup>7</sup>	4.3 × 10 <sup>4</sup>	8.0 × 10 <sup>6</sup>	3.8 × 10 <sup>8</sup>	3.0 × 10 <sup>3</sup>	2.4 × 10 <sup>4</sup>	9.4 × 10 <sup>3</sup>	7.6 × 10 <sup>4</sup>	2.5 × 10 <sup>3</sup>
	Max	5.2 × 10 <sup>7</sup>	2.5 × 10 <sup>5</sup>	2.1 × 10 <sup>7</sup>	9.5 × 10 <sup>8</sup>	1.8 × 10 <sup>4</sup>	6.1 × 10 <sup>8</sup>	1.0 × 10 <sup>5</sup>	5.4 × 10 <sup>5</sup>	1.5 × 10 <sup>4</sup>
	STD	1.2 × 10 <sup>7</sup>	6.4 × 10 <sup>4</sup>	5.0 × 10 <sup>6</sup>	2.0 × 10 <sup>8</sup>	6.3 × 10 <sup>3</sup>	1.9 × 10 <sup>8</sup>	2.8 × 10 <sup>4</sup>	1.3 × 10 <sup>5</sup>	4.5 × 10 <sup>3</sup>
	Rank	7	4	6	9	2	8	3	5	1
F <sub>14</sub>	Ave	8.0 × 10 <sup>4</sup>	4.7 × 10 <sup>5</sup>	1.9 × 10 <sup>4</sup>	2.1 × 10 <sup>5</sup>	1.8 × 10 <sup>3</sup>	7.1 × 10 <sup>4</sup>	6.2 × 10 <sup>4</sup>	2.9 × 10 <sup>5</sup>	1.7 × 10 <sup>3</sup>
	Min	1.6 × 10 <sup>4</sup>	1.6 × 10 <sup>4</sup>	4.2 × 10 <sup>3</sup>	4.6 × 10 <sup>4</sup>	1.6 × 10 <sup>3</sup>	1.7 × 10 <sup>4</sup>	2.4 × 10 <sup>4</sup>	3.7 × 10 <sup>4</sup>	1.6 × 10 <sup>3</sup>
	Max	2.5 × 10 <sup>5</sup>	2.0 × 10 <sup>6</sup>	3.2 × 10 <sup>4</sup>	5.6 × 10 <sup>5</sup>	3.2 × 10 <sup>3</sup>	1.4 × 10 <sup>5</sup>	1.0 × 10 <sup>5</sup>	8.3 × 10 <sup>5</sup>	1.7 × 10 <sup>3</sup>
	STD	7.0 × 10 <sup>4</sup>	6.1 × 10 <sup>5</sup>	7.9 × 10 <sup>3</sup>	1.9 × 10 <sup>5</sup>	5.0 × 10 <sup>2</sup>	3.9 × 10 <sup>4</sup>	2.6 × 10 <sup>4</sup>	2.3 × 10 <sup>5</sup>	4.9 × 10 <sup>1</sup>
	Rank	6	9	3	7	2	5	4	8	1
F <sub>15</sub>	Ave	4.9 × 10 <sup>5</sup>	9.5 × 10 <sup>4</sup>	1.8 × 10 <sup>6</sup>	2.0 × 10 <sup>7</sup>	1.2 × 10 <sup>4</sup>	2.1 × 10 <sup>4</sup>	2.3 × 10 <sup>4</sup>	7.6 × 10 <sup>4</sup>	2.5 × 10 <sup>3</sup>
	Min	1.4 × 10 <sup>5</sup>	1.7 × 10 <sup>4</sup>	9.3 × 10 <sup>5</sup>	1.9 × 10 <sup>6</sup>	1.9 × 10 <sup>3</sup>	1.6 × 10 <sup>4</sup>	7.5 × 10 <sup>3</sup>	3.1 × 10 <sup>4</sup>	1.6 × 10 <sup>3</sup>
	Max	1.1 × 10 <sup>6</sup>	1.9 × 10 <sup>5</sup>	2.6 × 10 <sup>6</sup>	4.4 × 10 <sup>7</sup>	4.0 × 10 <sup>4</sup>	4.4 × 10 <sup>4</sup>	5.9 × 10 <sup>4</sup>	1.5 × 10 <sup>5</sup>	5.3 × 10 <sup>3</sup>
	STD	2.7 × 10 <sup>5</sup>	5.0 × 10 <sup>4</sup>	6.3 × 10 <sup>5</sup>	1.2 × 10 <sup>7</sup>	1.3 × 10 <sup>4</sup>	8.9 × 10 <sup>3</sup>	1.7 × 10 <sup>4</sup>	3.8 × 10 <sup>4</sup>	1.3 × 10 <sup>3</sup>
	Rank	7	6	8	9	2	3	4	5	1
F <sub>16</sub>	Ave	2.6 × 10 <sup>3</sup>	3.3 × 10 <sup>3</sup>	2.9 × 10 <sup>3</sup>	3.8 × 10 <sup>3</sup>	2.7 × 10 <sup>3</sup>	3.9 × 10 <sup>3</sup>	2.6 × 10 <sup>3</sup>	3.1 × 10 <sup>3</sup>	2.4 × 10 <sup>3</sup>
	Min	2.3 × 10 <sup>3</sup>	2.5 × 10 <sup>3</sup>	2.4 × 10 <sup>3</sup>	3.5 × 10 <sup>3</sup>	2.4 × 10 <sup>3</sup>	3.0 × 10 <sup>3</sup>	2.0 × 10 <sup>3</sup>	2.6 × 10 <sup>3</sup>	2.1 × 10 <sup>3</sup>
	Max	2.8 × 10 <sup>3</sup>	3.8 × 10 <sup>3</sup>	3.3 × 10 <sup>3</sup>	4.0 × 10 <sup>3</sup>	3.1 × 10 <sup>3</sup>	4.8 × 10 <sup>3</sup>	3.2 × 10 <sup>3</sup>	4.0 × 10 <sup>3</sup>	2.6 × 10 <sup>3</sup>
	STD	1.9 × 10 <sup>2</sup>	4.3 × 10 <sup>2</sup>	2.6 × 10 <sup>2</sup>	1.6 × 10 <sup>2</sup>	2.5 × 10 <sup>2</sup>	5.2 × 10 <sup>2</sup>	3.7 × 10 <sup>2</sup>	4.1 × 10 <sup>2</sup>	1.9 × 10 <sup>2</sup>
	Rank	3	7	5	8	4	9	2	6	1
F <sub>17</sub>	Ave	2.0 × 10 <sup>3</sup>	2.5 × 10 <sup>3</sup>	2.1 × 10 <sup>3</sup>	2.5 × 10 <sup>3</sup>	2.3 × 10 <sup>3</sup>	2.7 × 10 <sup>3</sup>	2.2 × 10 <sup>3</sup>	2.3 × 10 <sup>3</sup>	2.1 × 10 <sup>3</sup>
	Min	1.9 × 10 <sup>3</sup>	2.1 × 10 <sup>3</sup>	2.0 × 10 <sup>3</sup>	2.3 × 10 <sup>3</sup>	2.0 × 10 <sup>3</sup>	2.5 × 10 <sup>3</sup>	2.0 × 10 <sup>3</sup>	1.8 × 10 <sup>3</sup>	1.9 × 10 <sup>3</sup>
	Max	2.1 × 10 <sup>3</sup>	2.9 × 10 <sup>3</sup>	2.3 × 10 <sup>3</sup>	2.7 × 10 <sup>3</sup>	2.7 × 10 <sup>3</sup>	3.2 × 10 <sup>3</sup>	2.3 × 10 <sup>3</sup>	2.6 × 10 <sup>3</sup>	2.3 × 10 <sup>3</sup>
	STD	7.7 × 10 <sup>1</sup>	2.4 × 10 <sup>2</sup>	1.0 × 10 <sup>2</sup>	1.7 × 10 <sup>2</sup>	2.5 × 10 <sup>2</sup>	2.6 × 10 <sup>2</sup>	9.6 × 10 <sup>1</sup>	2.4 × 10 <sup>2</sup>	1.6 × 10 <sup>2</sup>
	Rank	1	8	3	6	5	9	4	7	2

Table 3. Cont.

Function	Property	GWO	WOA	MVO	SCA	GBO	AOA	EO	AO	OLPSGBO
$F_{18}$	Ave	$1.3 \times 10^6$	$2.8 \times 10^6$	$3.3 \times 10^5$	$5.1 \times 10^6$	$3.3 \times 10^4$	$1.1 \times 10^6$	$4.0 \times 10^5$	$1.6 \times 10^6$	$1.7 \times 10^4$
	Min	$9.8 \times 10^4$	$2.7 \times 10^5$	$1.8 \times 10^5$	$2.8 \times 10^6$	$1.1 \times 10^4$	$1.6 \times 10^5$	$1.5 \times 10^5$	$2.2 \times 10^5$	$2.7 \times 10^3$
	Max	$7.2 \times 10^6$	$9.7 \times 10^6$	$4.6 \times 10^5$	$8.3 \times 10^6$	$9.4 \times 10^4$	$2.6 \times 10^6$	$7.7 \times 10^5$	$5.6 \times 10^6$	$3.3 \times 10^4$
	STD	$2.1 \times 10^6$	$3.1 \times 10^6$	$1.1 \times 10^5$	$1.7 \times 10^6$	$2.9 \times 10^4$	$6.7 \times 10^5$	$1.9 \times 10^5$	$2.0 \times 10^6$	$1.1 \times 10^4$
	Rank	5	8	3	9	2	6	4	7	1
$F_{19}$	Ave	$1.5 \times 10^6$	$2.8 \times 10^6$	$2.4 \times 10^6$	$3.8 \times 10^7$	$6.4 \times 10^3$	$2.7 \times 10^3$	$3.2 \times 10^4$	$8.0 \times 10^5$	$2.3 \times 10^3$
	Min	$3.0 \times 10^5$	$2.9 \times 10^5$	$1.2 \times 10^6$	$1.1 \times 10^7$	$2.0 \times 10^3$	$2.5 \times 10^3$	$3.2 \times 10^3$	$8.7 \times 10^4$	$2.0 \times 10^3$
	Max	$4.5 \times 10^6$	$7.4 \times 10^6$	$6.2 \times 10^6$	$8.6 \times 10^7$	$2.3 \times 10^4$	$2.9 \times 10^3$	$6.6 \times 10^4$	$1.8 \times 10^6$	$3.0 \times 10^3$
	STD	$1.2 \times 10^6$	$2.2 \times 10^6$	$1.4 \times 10^6$	$2.4 \times 10^7$	$6.1 \times 10^3$	$1.3 \times 10^2$	$2.5 \times 10^4$	$6.1 \times 10^5$	$2.6 \times 10^2$
	Rank	6	8	7	9	3	2	4	5	1
$F_{20}$	Ave	$2.4 \times 10^3$	$2.8 \times 10^3$	$2.5 \times 10^3$	$2.7 \times 10^3$	$2.4 \times 10^3$	$2.7 \times 10^3$	$2.4 \times 10^3$	$2.5 \times 10^3$	$2.3 \times 10^3$
	Min	$2.2 \times 10^3$	$2.4 \times 10^3$	$2.2 \times 10^3$	$2.5 \times 10^3$	$2.2 \times 10^3$	$2.5 \times 10^3$	$2.3 \times 10^3$	$2.2 \times 10^3$	$2.2 \times 10^3$
	Max	$2.7 \times 10^3$	$3.0 \times 10^3$	$2.9 \times 10^3$	$2.9 \times 10^3$	$2.5 \times 10^3$	$2.9 \times 10^3$	$2.8 \times 10^3$	$2.8 \times 10^3$	$2.5 \times 10^3$
	STD	$1.3 \times 10^2$	$1.9 \times 10^2$	$1.9 \times 10^2$	$1.3 \times 10^2$	$1.2 \times 10^2$	$1.1 \times 10^2$	$2.0 \times 10^2$	$1.8 \times 10^2$	$1.2 \times 10^2$
	Rank	3	9	6	8	2	7	4	5	1
$F_{21}$	Ave	$2.4 \times 10^3$	$2.5 \times 10^3$	$2.5 \times 10^3$	$2.6 \times 10^3$	$2.4 \times 10^3$	$2.6 \times 10^3$	$2.4 \times 10^3$	$2.5 \times 10^3$	$2.4 \times 10^3$
	Min	$2.4 \times 10^3$	$2.5 \times 10^3$	$2.4 \times 10^3$	$2.5 \times 10^3$	$2.4 \times 10^3$	$2.6 \times 10^3$	$2.4 \times 10^3$	$2.4 \times 10^3$	$2.4 \times 10^3$
	Max	$2.5 \times 10^3$	$2.7 \times 10^3$	$2.5 \times 10^3$	$2.6 \times 10^3$	$2.5 \times 10^3$	$2.6 \times 10^3$	$2.5 \times 10^3$	$2.5 \times 10^3$	$2.5 \times 10^3$
	STD	$2.7 \times 10^1$	$6.3 \times 10^1$	$2.7 \times 10^1$	$1.6 \times 10^1$	$3.0 \times 10^1$	$2.7 \times 10^1$	$4.0 \times 10^1$	$3.9 \times 10^1$	$4.1 \times 10^1$
	Rank	4	7	6	8	3	9	1	5	2
$F_{22}$	Ave	$4.3 \times 10^3$	$6.0 \times 10^3$	$6.8 \times 10^3$	$9.1 \times 10^3$	$3.2 \times 10^3$	$8.5 \times 10^3$	$6.1 \times 10^3$	$2.8 \times 10^3$	$2.3 \times 10^3$
	Min	$2.5 \times 10^3$	$2.3 \times 10^3$	$2.4 \times 10^3$	$4.0 \times 10^3$	$2.3 \times 10^3$	$6.7 \times 10^3$	$2.3 \times 10^3$	$2.3 \times 10^3$	$2.3 \times 10^3$
	Max	$7.5 \times 10^3$	$8.5 \times 10^3$	$9.7 \times 10^3$	$1.0 \times 10^4$	$8.0 \times 10^3$	$9.3 \times 10^3$	$7.9 \times 10^3$	$6.6 \times 10^3$	$2.3 \times 10^3$
	STD	$2.2 \times 10^3$	$2.5 \times 10^3$	$3.1 \times 10^3$	$1.8 \times 10^3$	$2.0 \times 10^3$	$7.3 \times 10^2$	$2.1 \times 10^3$	$1.4 \times 10^3$	$3.0 \times 10^1$
	Rank	4	5	7	9	3	8	6	2	1
$F_{23}$	Ave	$2.8 \times 10^3$	$3.1 \times 10^3$	$2.9 \times 10^3$	$3.0 \times 10^3$	$2.8 \times 10^3$	$3.4 \times 10^3$	$2.9 \times 10^3$	$2.8 \times 10^3$	$2.8 \times 10^3$
	Min	$2.8 \times 10^3$	$2.9 \times 10^3$	$2.8 \times 10^3$	$2.9 \times 10^3$	$2.7 \times 10^3$	$3.3 \times 10^3$	$2.7 \times 10^3$	$2.8 \times 10^3$	$2.8 \times 10^3$
	Max	$2.9 \times 10^3$	$3.3 \times 10^3$	$3.0 \times 10^3$	$3.0 \times 10^3$	$2.8 \times 10^3$	$3.6 \times 10^3$	$4.0 \times 10^3$	$2.9 \times 10^3$	$2.8 \times 10^3$
	STD	$1.7 \times 10^1$	$1.4 \times 10^3$	$4.9 \times 10^1$	$3.4 \times 10^1$	$2.8 \times 10^1$	$8.4 \times 10^1$	$3.9 \times 10^3$	$4.0 \times 10^1$	$1.3 \times 10^1$
	Rank	3	8	5	7	2	9	6	4	1
$F_{24}$	Ave	$3.0 \times 10^3$	$3.2 \times 10^3$	$3.0 \times 10^3$	$3.2 \times 10^3$	$3.0 \times 10^3$	$3.7 \times 10^3$	$3.0 \times 10^3$	$3.1 \times 10^3$	$2.9 \times 10^3$
	Min	$3.0 \times 10^3$	$3.1 \times 10^3$	$3.0 \times 10^3$	$3.1 \times 10^3$	$2.9 \times 10^3$	$3.6 \times 10^3$	$2.9 \times 10^3$	$2.9 \times 10^3$	$2.9 \times 10^3$
	Max	$3.0 \times 10^3$	$3.5 \times 10^3$	$3.0 \times 10^3$	$3.2 \times 10^3$	$3.0 \times 10^3$	$4.0 \times 10^3$	$3.9 \times 10^3$	$3.3 \times 10^3$	$3.0 \times 10^3$
	STD	$8.4 \times 10^1$	$1.5 \times 10^2$	$2.4 \times 10^1$	$3.4 \times 10^1$	$2.7 \times 10^1$	$1.4 \times 10^2$	$3.2 \times 10^2$	$9.9 \times 10^1$	$3.2 \times 10^1$
	Rank	4	7	3	8	2	9	5	6	1
$F_{25}$	Ave	$3.0 \times 10^3$	$2.9 \times 10^3$	$2.9 \times 10^3$	$3.2 \times 10^3$	$2.9 \times 10^3$	$4.5 \times 10^3$	$2.9 \times 10^3$	$2.9 \times 10^3$	$2.9 \times 10^3$
	Min	$2.9 \times 10^3$	$2.9 \times 10^3$	$2.9 \times 10^3$	$3.1 \times 10^3$	$2.9 \times 10^3$	$4.1 \times 10^3$	$2.9 \times 10^3$	$2.9 \times 10^3$	$2.9 \times 10^3$
	Max	$3.0 \times 10^3$	$2.9 \times 10^3$	$2.9 \times 10^3$	$3.3 \times 10^3$	$2.9 \times 10^3$	$5.4 \times 10^3$	$2.9 \times 10^3$	$2.9 \times 10^3$	$2.9 \times 10^3$
	STD	$3.0 \times 10^1$	$1.5 \times 10^1$	$1.0 \times 10^1$	$6.0 \times 10^1$	$9.8 \times 10^1$	$3.8 \times 10^2$	$1.5 \times 10^1$	$1.8 \times 10^1$	$9.0 \times 10^1$
	Rank	7	6	5	8	3	9	2	4	1

**Table 3.** Cont.

Function	Property	GWO	WOA	MVO	SCA	GBO	AOA	EO	AO	OLPSGBO
$F_{26}$	Ave	$5.4 \times 10^3$	$7.8 \times 10^3$	$5.2 \times 10^3$	$6.8 \times 10^3$	$4.8 \times 10^3$	$9.5 \times 10^3$	$4.9 \times 10^3$	$3.7 \times 10^3$	$4.6 \times 10^3$
	Min	$5.0 \times 10^3$	$6.2 \times 10^3$	$3.0 \times 10^3$	$5.0 \times 10^3$	$2.8 \times 10^3$	$8.0 \times 10^3$	$4.0 \times 10^3$	$2.9 \times 10^3$	$2.8 \times 10^3$
	Max	$5.7 \times 10^3$	$8.8 \times 10^3$	$6.0 \times 10^3$	$7.7 \times 10^3$	$5.7 \times 10^3$	$1.1 \times 1004$	$6.2 \times 10^3$	$5.3 \times 10^3$	$5.8 \times 10^3$
	STD	$2.0 \times 10^2$	$9.2 \times 10^2$	$1.1 \times 10^3$	$7.4 \times 10^2$	$1.0 \times 10^3$	$7.7 \times 10^2$	$7.3 \times 10^2$	$7.5 \times 10^2$	$1.3 \times 10^3$
	Rank	6	8	5	7	3	9	4	1	2
$F_{27}$	Ave	$3.3 \times 10^3$	$3.3 \times 10^3$	$3.2 \times 10^3$	$3.4 \times 10^3$	$3.2 \times 10^3$	$4.2 \times 10^3$	$3.2 \times 10^3$	$3.3 \times 10^3$	$3.2 \times 10^3$
	Min	$3.2 \times 10^3$	$3.3 \times 10^3$	$3.2 \times 10^3$	$3.3 \times 10^3$	$3.2 \times 10^3$	$3.9 \times 10^3$	$3.2 \times 10^3$	$3.2 \times 10^3$	$3.2 \times 10^3$
	Max	$3.3 \times 10^3$	$3.5 \times 10^3$	$3.2 \times 10^3$	$3.4 \times 10^3$	$3.3 \times 10^3$	$4.6 \times 10^3$	$3.3 \times 10^3$	$3.3 \times 10^3$	$3.3 \times 10^3$
	STD	$1.7 \times 10^1$	$7.6 \times 10^1$	$1.0 \times 10^1$	$2.6 \times 10^1$	$2.2 \times 10^1$	$2.2 \times 10^2$	$2.2 \times 10^1$	$2.6 \times 10^1$	$1.6 \times 10^1$
	Rank	5	7	1	8	4	9	3	6	2
$F_{28}$	Ave	$3.4 \times 10^3$	$3.3 \times 10^3$	$3.3 \times 10^3$	$4.0 \times 10^3$	$3.2 \times 10^3$	$6.3 \times 10^3$	$5.4 \times 10^3$	$3.3 \times 10^3$	$3.1 \times 10^3$
	Min	$3.3 \times 10^3$	$3.3 \times 10^3$	$3.2 \times 10^3$	$3.8 \times 10^3$	$3.1 \times 10^3$	$5.5 \times 10^3$	$3.2 \times 10^3$	$3.3 \times 10^3$	$3.1 \times 10^3$
	Max	$3.4 \times 10^3$	$3.3 \times 10^3$	$3.3 \times 10^3$	$4.3 \times 10^3$	$3.2 \times 10^3$	$7.5 \times 10^3$	$6.4 \times 10^3$	$3.4 \times 10^3$	$3.1 \times 10^3$
	STD	$3.3 \times 10^1$	$1.8 \times 10^1$	$2.1 \times 10^1$	$1.6 \times 10^2$	$6.1 \times 10^1$	$6.7 \times 10^2$	$1.5 \times 10^3$	$3.8 \times 10^1$	$2.6 \times 10^{-9}$
	Rank	6	3	5	7	2	9	8	4	1
$F_{29}$	Ave	$3.9 \times 10^3$	$5.0 \times 10^3$	$3.9 \times 10^3$	$4.7 \times 10^3$	$3.9 \times 10^3$	$6.3 \times 10^3$	$4.0 \times 10^3$	$4.3 \times 10^3$	$3.8 \times 10^3$
	Min	$3.6 \times 10^3$	$4.2 \times 10^3$	$3.7 \times 10^3$	$4.3 \times 10^3$	$3.6 \times 10^3$	$5.5 \times 10^3$	$3.8 \times 10^3$	$3.8 \times 10^3$	$3.5 \times 10^3$
	Max	$4.2 \times 10^3$	$5.9 \times 10^3$	$4.2 \times 10^3$	$5.1 \times 10^3$	$4.3 \times 10^3$	$7.5 \times 10^3$	$4.2 \times 10^3$	$4.8 \times 10^3$	$3.9 \times 10^3$
	STD	$1.6 \times 10^2$	$5.2 \times 10^2$	$1.6 \times 10^2$	$2.1 \times 10^2$	$2.2 \times 10^2$	$6.7 \times 10^2$	$1.4 \times 10^2$	$3.7 \times 10^2$	$1.4 \times 10^2$
	Rank	4	8	3	7	2	9	5	6	1
$F_{30}$	Ave	$8.0 \times 10^6$	$1.0 \times 10^7$	$4.1 \times 10^6$	$1.2 \times 10^8$	$7.7 \times 10^3$	$3.1 \times 10^7$	$1.4 \times 10^5$	$7.2 \times 10^6$	$6.1 \times 10^3$
	Min	$3.9 \times 10^6$	$1.6 \times 10^6$	$2.2 \times 10^6$	$6.1 \times 10^6$	$5.4 \times 10^3$	$5.3 \times 10^6$	$5.6 \times 10^3$	$3.4 \times 10^6$	$5.5 \times 10^3$
	Max	$1.3 \times 10^7$	$3.3 \times 10^7$	$9.6 \times 10^6$	$2.1 \times 10^8$	$1.4 \times 10^4$	$9.0 \times 10^7$	$7.3 \times 10^5$	$1.2 \times 10^7$	$6.5 \times 10^3$
	STD	$3.1 \times 10^6$	$8.9 \times 10^6$	$2.1 \times 10^6$	$5.2 \times 10^7$	$3.4 \times 10^3$	$2.4 \times 10^7$	$2.2 \times 10^5$	$2.9 \times 10^6$	$3.5 \times 10^2$
	Rank	6	7	4	9	2	8	3	5	1
Friedman average rank	4.9655	6.8966	4.931	7.8621	2.9655	7.7931	3.2414	4.8276	1.3793	
Friedman total rank	144	200	143	228	86	226	94	140	40	

**Table 4.** The Wilcoxon nonparametric statistical test (*p*-value).

Function	GWO	WOA	MVO	SCA	GBO	AOA	EO	AO
$F_1$	0.001953125	0.001953125	0.001953125	0.001953125	0.001953125	0.001953125	0.001953125	0.193359375
$F_2$	NA							
$F_3$	0.001953125	0.001953125	0.001953125	0.001953125	0.001953125	0.001953125	0.001953125	0.001953125
$F_4$	0.001953125	0.001953125	0.001953125	0.001953125	0.0078125	0.001953125	0.001953125	0.001953125
$F_5$	0.001953125	0.001953125	0.001953125	0.001953125	0.03125	0.001953125	0.001953125	0.013671875
$F_6$	0.275390625	0.001953125	0.064453125	0.001953125	0.01953125	0.001953125	0.001953125	0.001953125
$F_7$	0.001953125	0.001953125	0.001953125	0.001953125	0.0078125	0.001953125	0.001953125	0.001953125
$F_8$	0.01953125	0.001953125	0.001953125	0.001953125	0.193359375	0.001953125	0.00390625	0.232421875
$F_9$	0.4921875	0.001953125	0.130859375	0.001953125	0.193359375	0.001953125	0.001953125	0.001953125
$F_{10}$	0.001953125	0.001953125	0.001953125	0.001953125	0.048828125	0.001953125	0.921875	0.193359375
$F_{11}$	0.001953125	0.001953125	0.001953125	0.001953125	0.625	0.001953125	0.001953125	0.001953125

Table 4. Cont.

Function	GWO	WOA	MVO	SCA	GBO	AOA	EO	AO
$F_{12}$	0.001953125	0.001953125	0.001953125	0.001953125	0.845703125	0.001953125	0.001953125	0.001953125
$F_{13}$	0.001953125	0.001953125	0.001953125	0.001953125	0.556640625	0.001953125	0.00390625	0.001953125
$F_{14}$	0.001953125	0.001953125	0.001953125	0.001953125	0.625	0.001953125	0.001953125	0.001953125
$F_{15}$	0.001953125	0.001953125	0.001953125	0.001953125	0.001953125	0.001953125	0.001953125	0.001953125
$F_{16}$	0.064453125	0.001953125	0.00390625	0.001953125	0.01953125	0.001953125	0.130859375	0.001953125
$F_{17}$	0.064453125	0.013671875	0.845703125	0.009765625	0.275390625	0.001953125	0.625	0.01953125
$F_{18}$	0.001953125	0.001953125	0.001953125	0.001953125	0.375	0.001953125	0.001953125	0.001953125
$F_{19}$	0.001953125	0.001953125	0.001953125	0.001953125	0.009765625	0.013671875	0.001953125	0.001953125
$F_{20}$	1	0.00390625	0.01953125	0.001953125	0.921875	0.001953125	0.6953125	0.064453125
$F_{21}$	0.064453125	0.001953125	0.001953125	0.001953125	0.6953125	0.001953125	0.42578125	0.037109375
$F_{22}$	0.001953125	0.001953125	0.001953125	0.001953125	0.6875	0.001953125	0.001953125	0.001953125
$F_{23}$	0.001953125	0.001953125	0.001953125	0.001953125	0.4921875	0.001953125	0.6953125	0.009765625
$F_{24}$	0.001953125	0.001953125	0.048828125	0.001953125	0.048828125	0.001953125	0.625	0.01953125
$F_{25}$	0.001953125	0.00390625	0.009765625	0.001953125	0.275390625	0.001953125	0.921875	0.048828125
$F_{26}$	0.02734375	0.001953125	0.083984375	0.00390625	0.845703125	0.001953125	0.921875	0.064453125
$F_{27}$	0.048828125	0.001953125	0.375	0.001953125	0.4921875	0.001953125	0.556640625	0.00390625
$F_{28}$	0.001953125	0.001953125	0.001953125	0.001953125	0.232421875	0.001953125	0.001953125	0.001953125
$F_{29}$	0.037109375	0.001953125	0.16015625	0.001953125	0.375	0.001953125	0.048828125	0.005859375
$F_{30}$	0.001953125	0.001953125	0.001953125	0.001953125	0.322265625	0.001953125	0.00390625	0.001953125

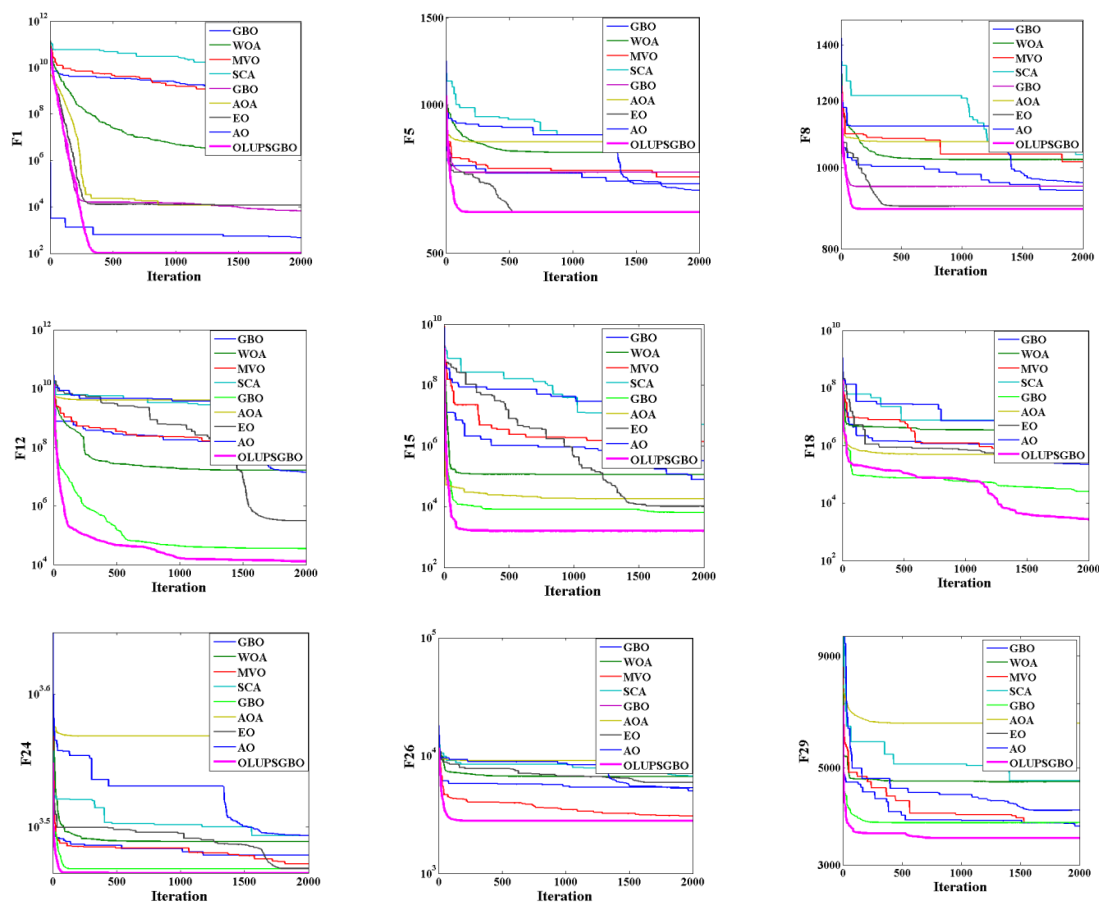


Figure 6. The convergence curves of some of the tested functions for illustration purposes.

#### 4. Inverse Analysis of Structural Damage Using the Developed Approach

Based on the theoretical background outlined in Section 2, this work utilizes the hybrid objective function in Equation (40). Physically, the objective function utilizes the  $MSEn$  and  $MKEn$  in order to derive the maximum dynamic characteristics related to the damage situation of the structure. The  $MSEn$  subobjective serves to identify the damage changes related to stiffness alterations of the structure and helps to identify linear damages in general, as well as to detect the occurrence of structural cracks based on the coupled effect of mode shapes and stiffness. In addition, the  $MKEn$  can contribute by coupling the effects of both natural modes, as well as mode shapes, together with any change in the mass matrix of the structure, which provides a prominent damage identifier and achieves a better generalized framework for damage diagnosis. In addition, with the help of modal assurance criterion, the mode shape-based subobjective in Equation (40) is also implemented in order to check the effect of damage on the mode shapes, regardless of the system stiffness and mass matrices, which helps in case of noisy conditions. To verify the performance of the proposed approach, the damage is considered to occur due to the reduction of stiffness corresponding to some selected damage scenarios of structural elements along the structure. The combination of the presented OL-UPSGBO algorithm and the new hybrid objective function, as well as their integration into the inverse analysis of structural damage identification problems, can be observed in Figure 7, as well as in the pseudo-code, as follows.

##### A. Initialization stage

1. Develop the FE model of the structure using a commercial software or a self-coded model.
2. Set a population of search agents, which are the damage indicators related to the overall structural or substructural elements, where each search agent represents one configuration of the FE model of the structure.
3. Extract the modal features related to the intact and damaged structure, and calculate the  $MSEn$ -,  $MKEn$ -, and mode shape-based sub-objectives using Equations (37)–(39). Thereafter, calculate the objective function using Equation (40) for each corresponding FE model configuration related to each candidate search agent.
4. Evaluate all the search agents using the developed objective function (as in Equation (40)).
5. Initialize all the stochastic parameters of the OL-UPSOGBO algorithm, as in Table 1.
6. Define the initial best global and local solutions, worst global solution, and the best performance of each search agent.
7. Apply the OL paradigm as in Equation (42).

##### B. Iterative stage

1. Start the UPSO framework by calculating the global and local velocities as in Equation (45).
2. Update the population using Equation (46).
3. Update the best global and local solutions, worst global solution, and the best performance of each search agent.
4. Start the GBO stage by employing Equation (61).
5. Apply the local escaping operator, as in Equation (63).
6. Apply the OL paradigm, as in Equation (42).
7. Update the best global and local solutions, worst global solution, and the best performance of each search agent.
8. Break if termination criteria are satisfied.

##### C. Damage identification stage

1. After termination of the iterative process, the best performed search agent is selected and registered.

2. The best solution contains the damage parameters  $\delta_j$  corresponding to each element  $j$ .
3. Elicit the damage locations and calculate the damage severities using Equation (41), and analyze the results.

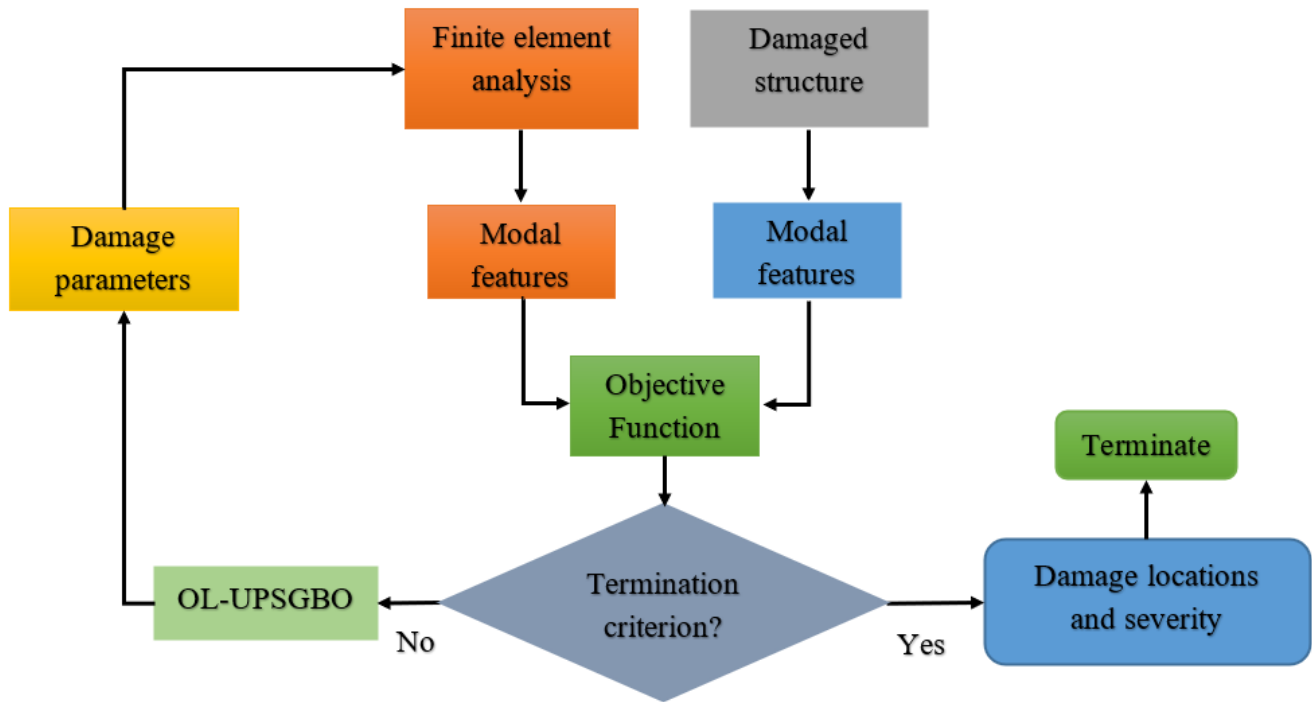
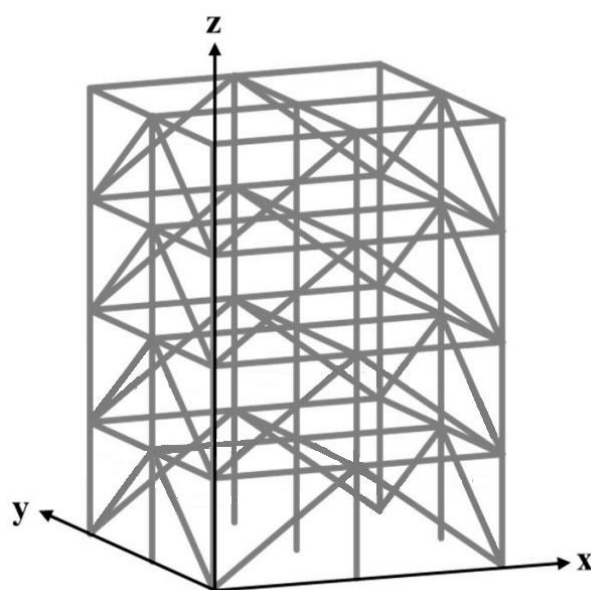


Figure 7. The pseudocode of the inverse analysis of structural damage using the proposed method.

To test the performance of the proposed approach for the inverse analysis of structural damage, the well-known American Society of Civil Engineering (ASCE) benchmark model is studied [67,68]. The frame model is widely utilized by the SHM society to study the robustness of damage identification approaches, as can be seen in [67,68]. The model is composed of four stories and 116 structural elements, as in Figure 8. To avoid the lengthy theoretical background, a complete explanation about the structural properties and physical parameters of the structure can be studied [67,68]. Hence, by utilizing the aforementioned structure, six damage scenarios are considered in this paper, which can provide the big picture regarding the efficiency of the developed approach. The six scenarios were made by reducing the structural stiffness of some selected brace elements by 25%. Such a small damage severity can be challenging to detect and localize using traditional approaches, as it has a small effect on structural responses. Additionally, the modal responses of one damage scenario, which is scenario 6, are subjected to two levels of Gaussian noise, specifically 3% and 5%. Furthermore, in this work, incomplete modal data which contains maximum dynamic information, are considered to better simulate practical engineering. The six damage scenarios are written as in Table 5.

Table 5. Damage scenarios.

Damage Scenario	Damage Locations	Damage Severity
Scenario 1	Brace elements 83, and 114	25%
Scenario 2	Brace elements 26, and 55	25%
Scenario 3	Brace elements 52, and 109	25%
Scenario 4	Brace elements 24, 82, and 112	25%
Scenario 5	Brace elements 23, 51, and 111	25%
Scenario 6	Brace elements 22, 51, 80, and 109	25%



**Figure 8.** The American Society of Civil Engineering benchmark frame structure [67,68].

The proposed method has the remarkable merits of utilizing several search mechanisms that are able to overcome the multimodal and complex optimization features of the problem of inverse analysis of structural damage with very few stochastic parameter settings. Using the stochastic parameters in Table 2, several population sizes were first tested and a population size of 100 search agents was selected. The performance of the proposed OL-UPSGBO algorithm is compared with the component algorithms, namely the UPSO and the GBO. Each algorithm is run 10 times after considering the high computational time required to solve the inverse analysis of the structural damage problem. Two types of statistical tests are conducted, which are the parametric tests, using the mean, minimum, maximum, and standard deviation of solutions, and the non-parametric test, using the well-known Wilcoxon Sign Rank Test [62]. The results of the inverse analysis of the structural damage problem are shown in Table 6. Moreover, the detailed damage identification results and the evolution of damage parameters of the considered elements related to damage scenarios 1, 2, 3, 4, 5, and 6 are shown in Figures 9–14. In addition, the noise immunity of the proposed approach can be seen in Figures 15 and 16, where the two noisy conditions of 3% and 5% Gaussian noise of scenario 6 are illustrated. By studying Table 6, it is well-observed that the proposed OL-UPSGBO algorithm has shown great performance when employed to solve the new hybrid objective function, with remarkable damage identification abilities even under noisy conditions. The  $p$ -value taken from the Wilcoxon test is under the confidence level of 0.05, which proves the statistical significance of the OL-UPSGBO algorithm compared to the UPSO and GBO algorithms.

The reason why the proposed OL-UPSGBO has shown an outstanding performance is because the main global search paradigm of GBO is improved by using two search mechanisms, namely by oppositional-based learning (OL), which is able to evaluate the oppositional of a considered solution and compares the two solutions in order to choose a better one. This efficient tool helps to accelerate the convergence of the algorithm and explore more search areas, which suits problems concerning multimodality and multiple local optima of the inverse problem of structural damage identification. In particular, the use of OL in both initialization and iterative phases has a major effect on boosting the exploration and exploitation of the algorithm. In addition, the local search mechanism of the powerful UPSO has been incorporated with the main computational framework of the GBO. This ensemble framework can boost the local search ability of GBO and provide a robust optimizer to deal with the high computationally-consuming and ill-posed problem of the inverse analysis of structural damage.

**Table 6.** Inverse analysis of structural damage using the proposed method.

Damage Scenario	Algorithm	Mean	Standard Deviation	Min	Max	Wilcoxon Sign Rank ( <i>p</i> -Value)
Scenario 1	UPSO	$5.7 \times 10^{-4}$	$5.7 \times 10^{-4}$	$6.5 \times 10^{-6}$	$1.2 \times 10^{-3}$	$3.9 \times 10^{-3}$
	GBO	$6.3 \times 10^{-3}$	$2.3 \times 10^{-4}$	$6.1 \times 10^{-3}$	$6.5 \times 10^{-3}$	$9.0 \times 10^{-3}$
	OL-UPSGBO	$1.1 \times 10^{-6}$	$2.2 \times 10^{-6}$	$6.2 \times 10^{-7}$	$6.5 \times 10^{-6}$	
Scenario 2	UPSO	$1.3 \times 10^{-2}$	$1.4 \times 10^{-5}$	$1.3 \times 10^{-2}$	$1.3 \times 10^{-2}$	$9.0 \times 10^{-3}$
	GBO	$1.6 \times 10^{-2}$	$4.8 \times 10^{-3}$	$1.1 \times 10^{-2}$	$2.1 \times 10^{-2}$	$9.0 \times 10^{-3}$
	OL-UPSGBO	$9.3 \times 10^{-8}$	$1.1 \times 10^{-7}$	$4.9 \times 10^{-7}$	$2.8 \times 10^{-7}$	
Scenario 3	UPSO	$5.3 \times 10^{-3}$	$1.1 \times 10^{-4}$	$5.2 \times 10^{-3}$	$5.4 \times 10^{-3}$	$9.0 \times 10^{-3}$
	GBO	$6.8 \times 10^{-2}$	$5.4 \times 10^{-4}$	$6.8 \times 10^{-2}$	$6.9 \times 10^{-2}$	$3.9 \times 10^{-3}$
	OL-UPSGBO	$5.5 \times 10^{-7}$	$8.2 \times 10^{-7}$	$3.2 \times 10^{-8}$	$2.0 \times 10^{-6}$	
Scenario 4	UPSO	$1.3 \times 10^{-2}$	$3.0 \times 10^{-5}$	$1.3 \times 10^{-2}$	$1.3 \times 10^{-2}$	$3.9 \times 10^{-3}$
	GBO	$5.3 \times 10^{-2}$	$1.7 \times 10^{-2}$	$4.1 \times 10^{-2}$	$7.6 \times 10^{-2}$	$3.9 \times 10^{-3}$
	OL-UPSGBO	$3.9 \times 10^{-6}$	$4.6 \times 10^{-6}$	$8.8 \times 10^{-8}$	$1.2 \times 10^{-5}$	
Scenario 5	UPSO	$3.5 \times 10^{-2}$	$3.7 \times 10^{-4}$	$3.5 \times 10^{-2}$	$3.5 \times 10^{-2}$	$3.9 \times 10^{-3}$
	GBO	$2.8 \times 10^{-2}$	$1.9 \times 10^{-3}$	$2.7 \times 10^{-2}$	$3.3 \times 10^{-2}$	$9.1 \times 10^{-3}$
	OL-UPSGBO	$2.2 \times 10^{-5}$	$3.1 \times 10^{-6}$	$1.9 \times 10^{-5}$	$2.6 \times 10^{-5}$	
Scenario 6	UPSO	$1.3 \times 10^{-2}$	$1.9 \times 10^{-5}$	$1.3 \times 10^{-2}$	$1.3 \times 10^{-2}$	$3.9 \times 10^{-3}$
	GBO	$2.3 \times 10^{-2}$	$7.3 \times 10^{-4}$	$2.3 \times 10^{-2}$	$2.4 \times 10^{-2}$	$3.9 \times 10^{-3}$
	OL-UPSGBO	$1.6 \times 10^{-6}$	$1.9 \times 10^{-6}$	$1.9 \times 10^{-8}$	$5.2 \times 10^{-6}$	
Scenario 6 (3% noise)	UPSO	$1.3 \times 10^{-2}$	$2.5 \times 10^{-5}$	$1.3 \times 10^{-2}$	$1.3 \times 10^{-2}$	$3.9 \times 10^{-3}$
	GBO	$2.5 \times 10^{-2}$	$1.1 \times 10^{-5}$	$2.5 \times 10^{-2}$	$2.5 \times 10^{-2}$	$3.9 \times 10^{-3}$
	OL-UPSGBO	$4.0 \times 10^{-4}$	$7.5 \times 10^{-7}$	$4.0 \times 10^{-4}$	$4.0 \times 10^{-4}$	
Scenario 6 (5% noise)	UPSO	$1.3 \times 10^{-2}$	$2.7 \times 10^{-5}$	$1.3 \times 10^{-2}$	$1.3 \times 10^{-2}$	$3.9 \times 10^{-3}$
	GBO	$2.5 \times 10^{-2}$	$5.3 \times 10^{-4}$	$2.5 \times 10^2$	$2.6 \times 10^{-4}$	$3.9 \times 10^{-3}$
	OL-UPSGBO	$5.8 \times 10^{-4}$	$4.0 \times 10^{-6}$	$5.8 \times 10^{-4}$	$5.9 \times 10^{-4}$	

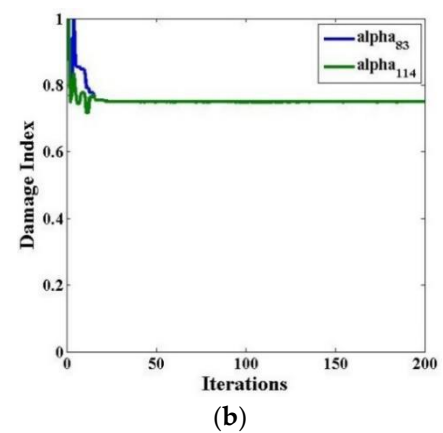
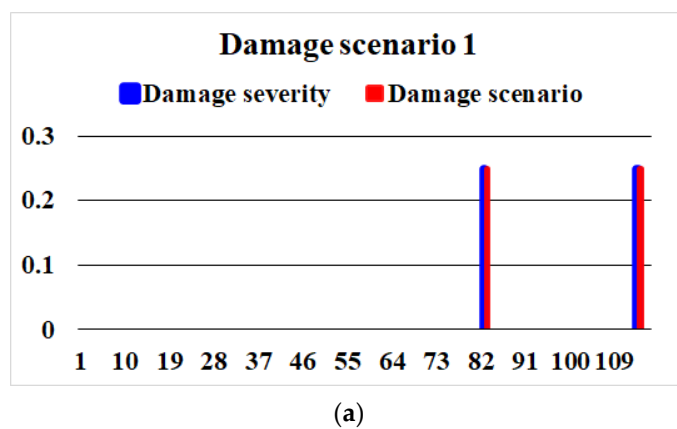
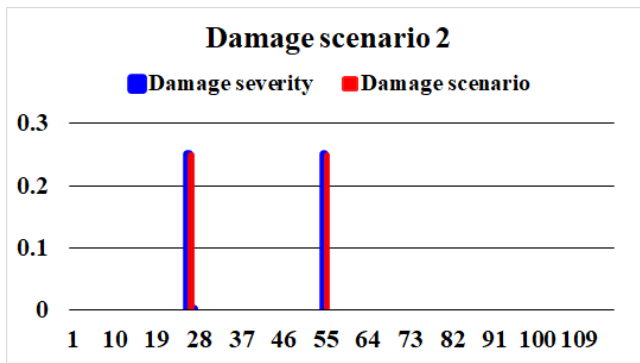
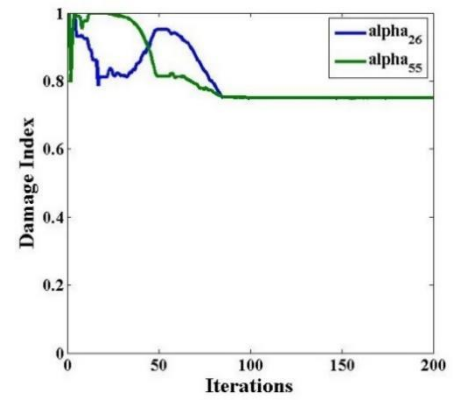


**Figure 9.** Damage identification for Scenario 1: (a) Damage locations and severity, and (b) convergence of damage parameters related to damaged elements.

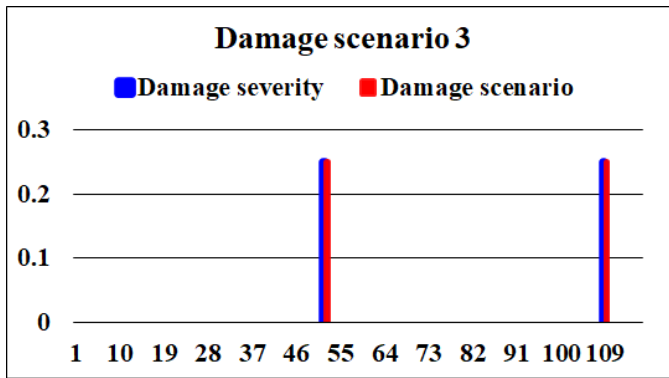


(a)

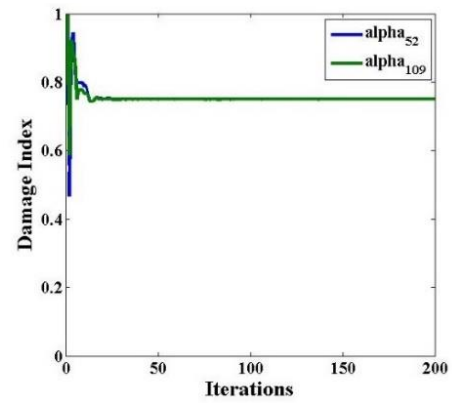


(b)

Figure 10. Damage identification for Scenario 2: (a) Damage locations and severity, and (b) convergence of damage parameters related to damaged elements.

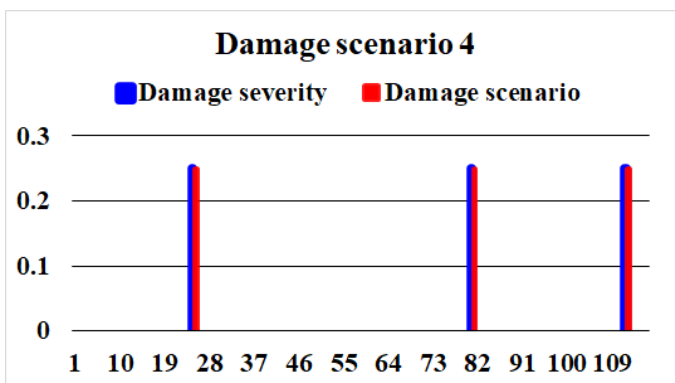


(a)

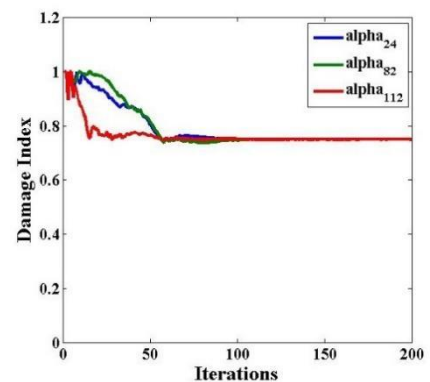


(b)

Figure 11. Damage identification for Scenario 3: (a) Damage locations and severity, and (b) convergence of damage parameters related to damaged elements.

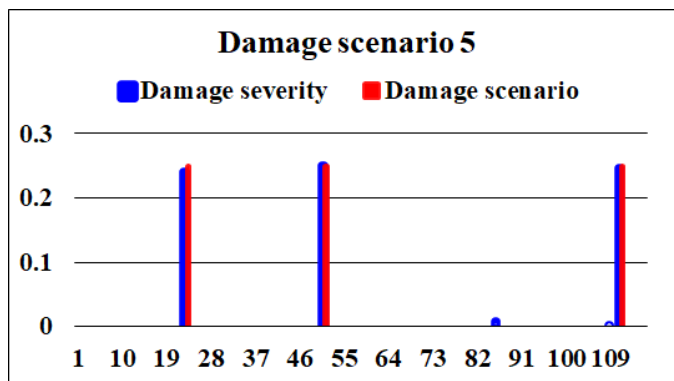


(a)

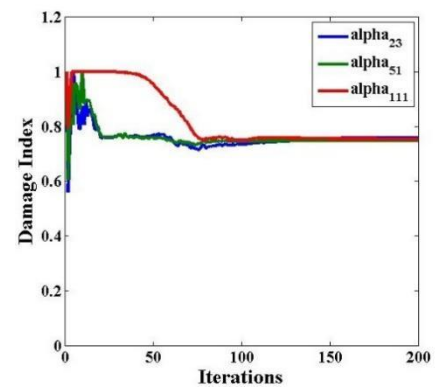


(b)

Figure 12. Damage identification for Scenario 4: (a) Damage locations and severity, and (b) convergence of damage parameters related to damaged elements.

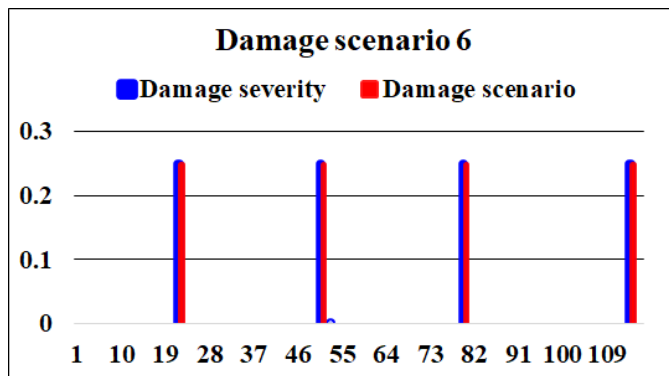


(a)

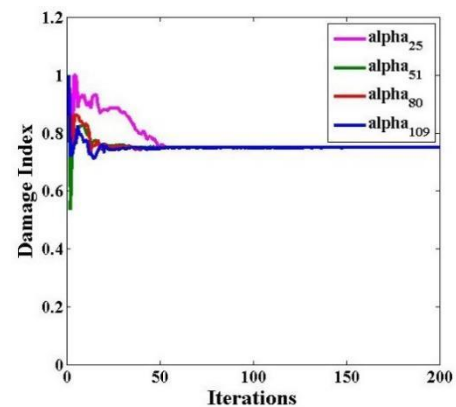


(b)

Figure 13. Damage identification for Scenario 5: (a) Damage locations and severity, and (b) convergence of damage parameters related to damaged elements.

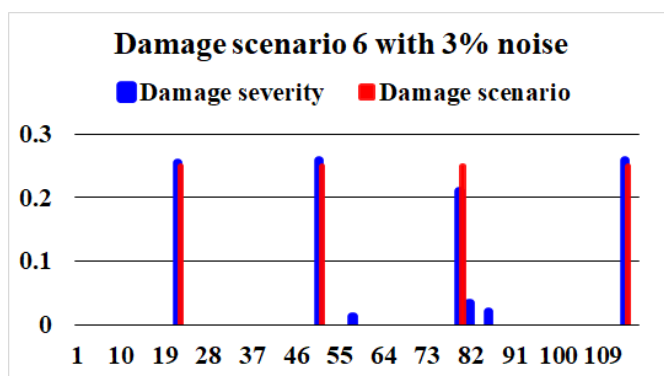


(a)

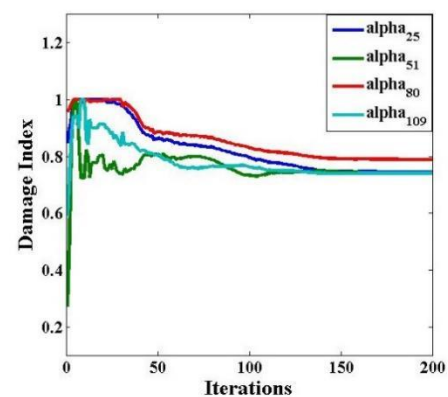


(b)

Figure 14. Damage identification for Scenario 6: (a) Damage locations and severity, and (b) convergence of damage parameters related to damaged elements.



(a)



(b)

Figure 15. Damage identification for Scenario 6 with 3% noise: (a) Damage locations and severity, and (b) convergence of damage parameters related to damaged elements.

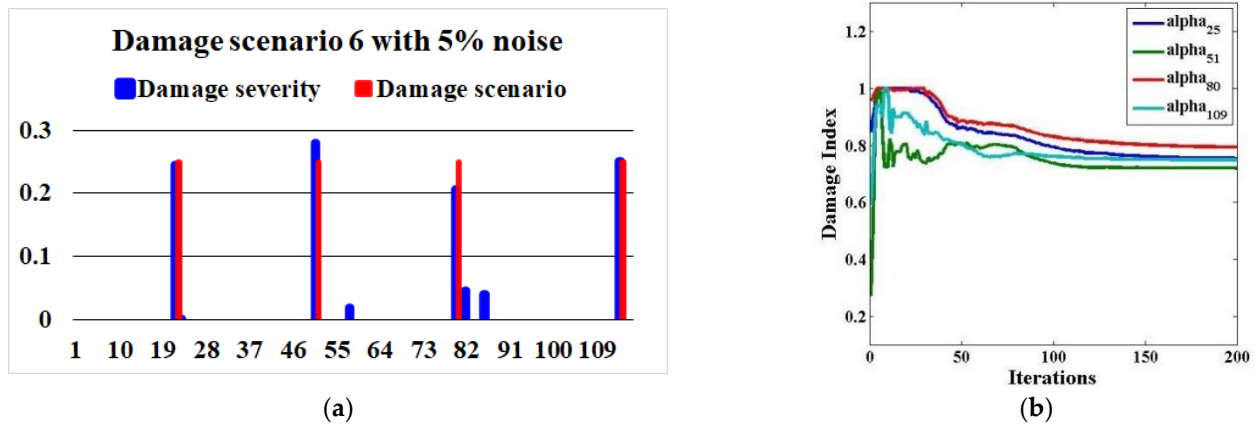


Figure 16. Damage identification for Scenario 6 with 5% noise: (a) Damage locations and severity, and (b) convergence of damage parameters related to damaged elements.

Even though the use of more than one modal property contributes to improve the overall damage identification, where each property helps to discover more underlying damage information, the contribution of each modal property used in the objective function should be studied. In order to further verify the developed approach and the robustness of the proposed objective function, a comparison with component sub-objectives is conducted separately using each of the three sub-objectives. In particular, the inverse analysis of damage identification problems is conducted using the MSEN, MKEn, and mode shape sub-objectives in Equations (7), (10), and (11), respectively. The most challenging multi-damage scenario, scenario 6, is studied. The damage identification results using the MSEN, MSEN, MKEn, and mode shape sub-objectives can be observed in Figures 17–19, respectively. From Figure 17, it is obvious that the MSEN sub-objective alone has helped to identify the damage in elements 51 and 80 with several damage identification errors along the structure. Additionally, in Figure 18, the MKEn sub-objective has contributed to identifying damage in elements 25 and 51, with high values of errors in some other locations. Lastly, the mode shape objective function has achieved damage identification in elements 80 and 109. It is clear that the overall three sub-objectives have contributed to identifying the overall damage in all elements and improved the damage severity determination when the case of multiple damage is studied.

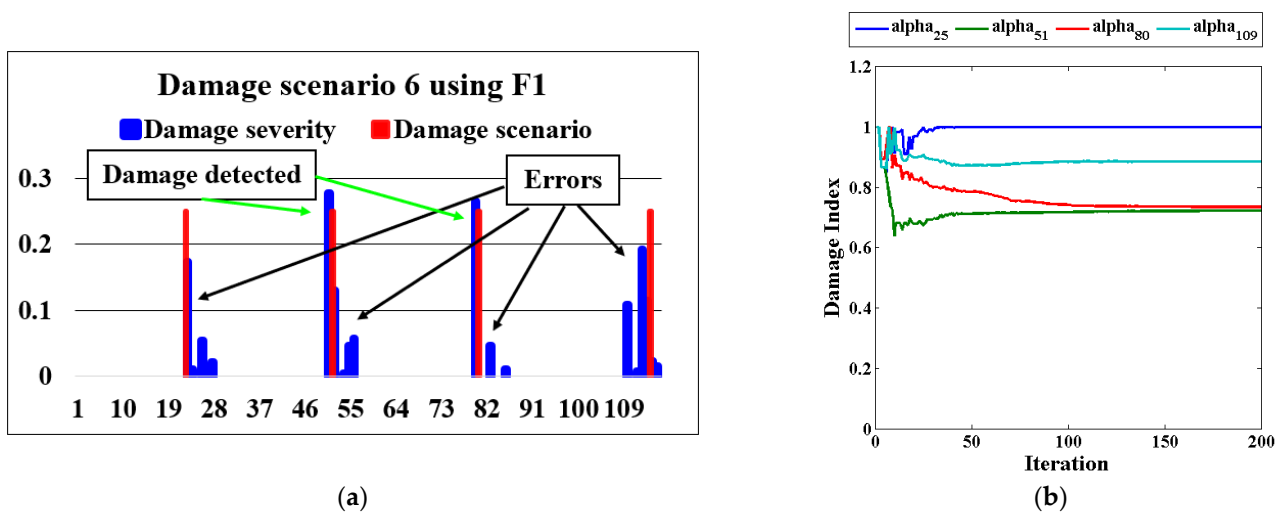
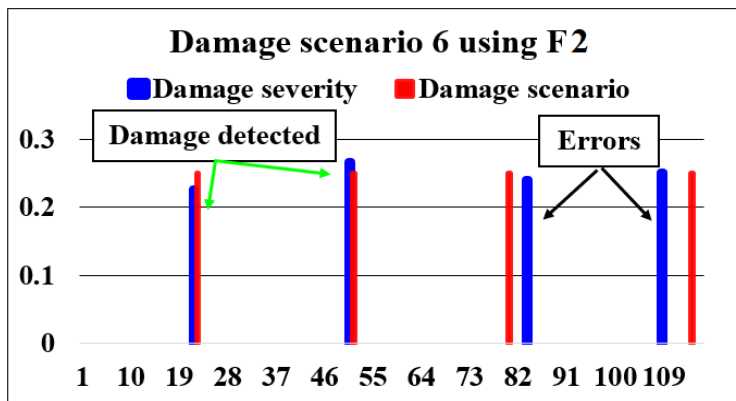
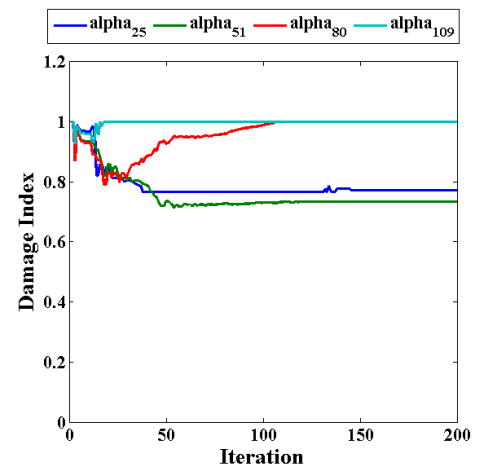


Figure 17. Damage identification for Scenario 6 using  $F_1$ : (a) Damage locations and severity, and (b) convergence of damage parameters related to damaged elements.

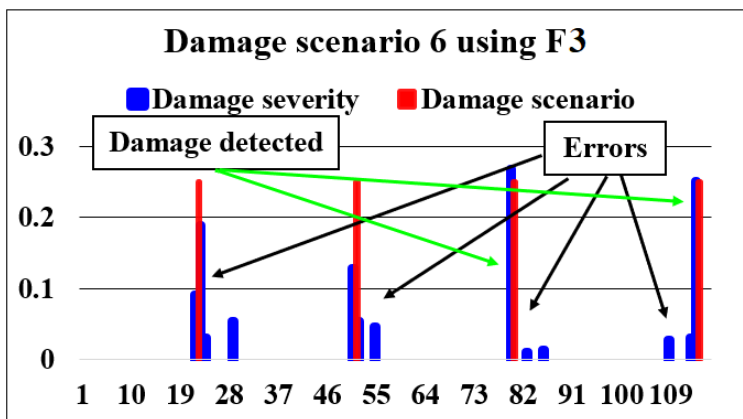


(a)

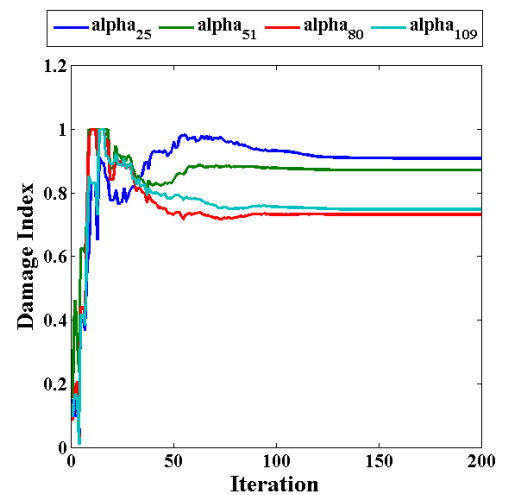


(b)

Figure 18. Damage identification for Scenario 6 using  $F_2$ : (a) Damage locations and severity, and (b) convergence of damage parameters related to damaged elements.



(a)



(b)

Figure 19. Damage identification for Scenario 6 using  $F_3$ : (a) Damage locations and severity, and (b) convergence of damage parameters related to damaged elements.

### 5. Conclusions

This study has discussed an efficient approach for solving the inverse analysis of structural damage problem using a new framework based on a new modal feature-based objective function, as well as a new evolutionary computation algorithm. The new hybrid objective function was formulated based on the modal strain and modal kinetic energy terms, which helps to contrast the maximum modal information from the structure under consideration. Moreover, in order to improve noise immunity and separate the modal responses from system matrices, which helps to cover more damage types, the modal assurance criterion of mode shapes was utilized and added as a third term to the objective function. In addition, to overcome the complex nature of the considered inverse problem, the OL framework for population initialization and convergence acceleration was first adopted. Thereafter, the UPSO elitism mechanism was merged with the efficient search mechanisms of the GBO. The newly developed algorithm OL-UPSGBO, with the characteristics of the convergence acceleration feature of OL, enhanced balanced exploration-exploitation of UPSO, and the local escaping operator of GBO was designed and tested. The OL-UPSGBO was tested using the CEC 2017, the most complex and well-known benchmark objective func-

tion set containing unimodal, multimodal, hybrid, and composite objective functions, and was compared to available state-of-the-art algorithms in the literature. The benchmarking results showed a remarkable performance of the proposed OL-UPSGBO algorithm compared to other approaches. Furthermore, as the main aim of this study, the proposed algorithm was implemented to solve the new hybrid objective function related to the inverse problem of structural damage detection. The ASCE frame structure was studied and several damage scenarios were tested. Compared to the component algorithms, the OL-UPSGBO algorithm showed a robust and stable computational performance, and remarkable damage deductibility for all damage scenarios even under noisy conditions. This can be well-observed by the parametric and non-parametric statistical tests after executing the damage identification framework. Hence, the developed approach can be highly recommended to solve the inverse analysis of structural damage problem.

**Author Contributions:** Conceptualization, N.F.A. and L.S.; methodology, N.F.A.; software, N.F.A.; validation, N.F.A., L.S., T.A.-h., X.Q. and M.C.; formal analysis, N.F.A., L.S. and T.A.-h.; investigation, N.F.A., L.S. and T.A.-h.; resources, N.F.A.; data curation, N.F.A. and T.A.-h.; writing—original draft preparation, N.F.A.; writing—review and editing, N.F.A.; visualization, N.F.A.; supervision, X.Q. and M.C.; project administration, X.Q., and M.C.; funding acquisition, X.Q. and M.C. All authors have read and agreed to the published version of the manuscript.

**Funding:** This research was funded by the Research Fund for International Young Scientists of the National Natural Science Foundation of China (No. 52250410359), the 2022 National Young Foreign Talents Program of China (No. QN2022143002L), the Fundamental Research Funds for the Central Universities (No. B220204002), and the Anhui Provincial International Joint Research Center of Data Diagnosis and Smart Maintenance on Bridge Structures (No. 2021AHGHZD01).

**Institutional Review Board Statement:** Not applicable.

**Informed Consent Statement:** Not applicable.

**Data Availability Statement:** Data sharing does not apply to this article as no datasets were generated or analyzed during the current study.

**Conflicts of Interest:** The authors declare no conflict of interest.

## References

1. Toh, G.; Park, J. Review of vibration-based structural health monitoring using deep learning. *Appl. Sci.* **2020**, *10*, 1680. [[CrossRef](#)]
2. Moughty, J.J.; Casas, J.R. A state of the art review of modal-based damage detection in bridges: Development, challenges and solutions. *Appl. Sci.* **2017**, *7*, 510. [[CrossRef](#)]
3. Dolati, S.S.K.; Caluk, N.; Mehrabi, A.; Dolati, S.S.K. Non-destructive testing applications for steel bridges. *Appl. Sci.* **2021**, *11*, 9757. [[CrossRef](#)]
4. Caicedo, D.; Lara-Valencia, L.; Valencia, Y. Machine learning techniques and population-based metaheuristics for damage detection and localization through frequency and modal-based structural health monitoring: A review. *Arch. Comput. Methods Eng.* **2022**, *29*, 3541–3565. [[CrossRef](#)]
5. Alkayem, N.F.; Cao, M.; Zhang, Y.; Bayat, M.; Su, Z. Structural damage detection using finite element model updating with evolutionary algorithms: A survey. *Neural Comput. Appl.* **2018**, *30*, 389–411. [[CrossRef](#)] [[PubMed](#)]
6. Minh, H.-L.; Sang-To, T.; Wahab, M.A.; Cuong-Le, T. Structural damage identification in thin-shell structures using a new technique combining finite element model updating and improved Cuckoo search algorithm. *Adv. Eng. Softw.* **2022**, *173*, 103206. [[CrossRef](#)]
7. Minh, H.-L.; Sang-To, T.; Wahab, M.A.; Cuong-Le, T. A new metaheuristic optimization based on K-means clustering algorithm and its application to structural damage identification. *Knowl.-Based Syst.* **2022**, *251*, 109189. [[CrossRef](#)]
8. Ereiz, S.; Duvnjak, I.; Jiménez-Alonso, J.F. Review of finite element model updating methods for structural applications. *Structures* **2022**, *41*, 684–723. [[CrossRef](#)]
9. Lu, Z.; Lv, Y.; Ouyang, H. A super-harmonic feature based updating method for crack identification in rotors using a kriging surrogate model. *Appl. Sci.* **2019**, *9*, 2428. [[CrossRef](#)]
10. Ereiz, S.; Duvnjak, I.; Jiménez-Alonso, J.F. Structural finite element model updating optimization based on game theory. *Mater. Today Proc.* **2022**, *65*, 1425–1432. [[CrossRef](#)]
11. Ding, Z.; Hou, R.; Xia, Y. Structural damage identification considering uncertainties based on a Jaya algorithm with a local pattern search strategy and L0.5 sparse regularization. *Eng. Struct.* **2022**, *261*, 114312. [[CrossRef](#)]

12. Ding, Z.; Li, J.; Hao, H. Simultaneous identification of structural damage and nonlinear hysteresis parameters by an evolutionary algorithm-based artificial neural network. *Int. J. Non-Linear Mech.* **2022**, *142*, 103970. [[CrossRef](#)]
13. Al-Hababi, T.; Al-Kayem, N.F.; Cui, L.; Zhang, S.; Liu, C.; Cao, M. The coupled effect of temperature changes and damage depth on natural frequencies in beam-like structures. *Struct. Durab. Health Monit.* **2022**, *16*, 15–35. [[CrossRef](#)]
14. Al-Hababi, T.; Cao, M.; Al-Kayem, N.F.; Shi, B.; Wei, Q.; Cui, L.; Šumarac, D.; Ragulskis, M. The dual Fourier transform spectra (DFTS): A new nonlinear damage indicator for identification of breathing cracks in beam-like structures. *Nonlinear Dyn.* **2022**, 1–23. [[CrossRef](#)]
15. Al-Hababi, T.; Al-Kayem, N.F.; Zhu, H.; Cui, L.; Zhang, S.; Cao, M. Effective identification and localization of single and multiple breathing cracks in beams under gaussian excitation using time-domain analysis. *Mathematics* **2022**, *10*, 1853. [[CrossRef](#)]
16. Al-Hababi, T.; Cao, M.; Saleh, B.; Alkayem, N.F.; Xu, H. A critical review of nonlinear damping identification in structural dynamics: Methods, applications, and challenges. *Sensors* **2020**, *20*, 7303. [[CrossRef](#)]
17. Yang, X.; Ouyang, H.; Guo, X.; Cao, S. Modal strain energy-based model updating method for damage identification on beam-like structures. *J. Struct. Eng.* **2020**, *146*, 04020246. [[CrossRef](#)]
18. Wang, N.; Zhu, R.-H.; Wang, Q.-M.; Zheng, J.-H.; Zhang, J.-B. A method for quantitative damage identification in a high-piled wharf based on modal strain energy residual variability. *Ocean Eng.* **2022**, *254*, 111314. [[CrossRef](#)]
19. Moradipour, P.; Chan, T.H.; Gallage, C. Benchmark studies for bridge health monitoring using an improved modal strain energy method. *Procedia Eng.* **2017**, *188*, 194–200. [[CrossRef](#)]
20. Yan, W.-J.; Ren, W.-X. A direct algebraic method to calculate the sensitivity of element modal strain energy. *Int. J. Numer. Methods Biomed. Eng.* **2011**, *27*, 694–710. [[CrossRef](#)]
21. Entezami, A.; Shariatmadar, H. Damage detection in structural systems by improved sensitivity of modal strain energy and Tikhonov regularization method. *Int. J. Dyn. Control* **2014**, *2*, 509–520. [[CrossRef](#)]
22. Vo-Duy, T.; Ho-Huu, V.; Dang-Trung, H.; Nguyen-Thoi, T. A two-step approach for damage detection in laminated composite structures using modal strain energy method and an improved differential evolution algorithm. *Compos. Struct.* **2016**, *147*, 42–53. [[CrossRef](#)]
23. Dinh-Cong, D.; Nguyen-Thoi, T.; Nguyen, D.T. A two-stage multi-damage detection approach for composite structures using MKECR-Tikhonov regularization iterative method and model updating procedure. *Appl. Math. Model.* **2021**, *90*, 114–130. [[CrossRef](#)]
24. Dinh-Cong, D.; Nguyen-Thoi, T.; Vinyas, M.; Nguyen, D.T. Two-stage structural damage assessment by combining modal kinetic energy change with symbiotic organisms search. *Int. J. Struct. Stab. Dyn.* **2019**, *19*, 1950120. [[CrossRef](#)]
25. Joseph, J.T.; Chan, T.H.T.; Nguyen, K.-D. Correlation-based damage identification and quantification using modal kinetic energy change. *Int. J. Struct. Stab. Dyn.* **2020**, *20*, 2042007. [[CrossRef](#)]
26. Joseph, J.T.; Chan, T.H.T.; Nguyen, A.; Nguyen, K.D. Damage identification of civil structures using modal kinetic energy change approach. In *ACMSM25. Lecture Notes in Civil Engineering*; Wang, C., Ho, J., Kitipornchai, S., Eds.; Springer: Singapore, 2020; Volume 37.
27. Pooya, S.M.H.; Massumi, A. A novel damage detection method in beam-like structures based on the relation between modal kinetic energy and modal strain energy and using only damaged structure data. *J. Sound Vib.* **2022**, *530*, 116943. [[CrossRef](#)]
28. Torkzadeh, P.; Goodarzi, Y.; Salajegheh, E. A two-stage damage detection method for large-scale structures by kinetic and modal strain energies using heuristic particle swarm optimization. *Int. J. Optim. Civ. Eng.* **2013**, *3*, 465–482.
29. Xu, M.; Wang, S.; Jiang, Y. Structural damage identification by a cross modal energy sensitivity based mode subset selection strategy. *Mar. Struct.* **2021**, *77*, 102968. [[CrossRef](#)]
30. Shahri, A.H.; Ghorbani-Tanha, A. Damage detection via closed-form sensitivity matrix of modal kinetic energy change ratio. *J. Sound Vib.* **2017**, *401*, 268–281. [[CrossRef](#)]
31. Gomes, G.F.; Mendez, Y.A.D.; da Silva Lopes Alexandrino, P.; da Cunha, S.S.; Anceletti, A.C. A review of vibration based inverse methods for damage detection and identification in mechanical structures using optimization algorithms and ANN. *Arch. Comput. Methods Eng.* **2019**, *26*, 883–897. [[CrossRef](#)]
32. Jafarkhani, R.; Masri, S.F. Finite element model updating using evolutionary strategy for damage detection. *Comput.-Aided Civ. Infrastruct. Eng.* **2011**, *26*, 207–224. [[CrossRef](#)]
33. Kaveh, A.; Hosseini, S.M.; Zaeerza, A. A physics-based metaheuristic algorithm based on Doppler effect phenomenon and mean euclidian distance threshold. *Period. Polytech. Civ. Eng.* **2022**, *66*, 820–842. [[CrossRef](#)]
34. Wang, G.-G.; Deb, S.; Coelho, L.d.S. Elephant herding optimization. In Proceedings of the 3rd International Symposium on Computational and Business Intelligence (ISCBI), Bali, Indonesia, 7–9 December 2015.
35. Wang, G.-G. Moth search algorithm: A bio-inspired metaheuristic algorithm for global optimization problems. *Memetic Comput.* **2018**, *10*, 151–164. [[CrossRef](#)]
36. Parsopoulos, K.E.; Vrahatis, M.N. Unified particle swarm optimization for solving constrained engineering optimization problems. In *Advances in Natural Computation. ICNC 2005. Lecture Notes in Computer Science*; Wang, L., Chen, K., Ong, Y.S., Eds.; Springer: Berlin/Heidelberg, Germany, 2005; Volume 3612.
37. Ghannadi, P.; Kourehli, S.S. Efficiency of the slime mold algorithm for damage detection of large-scale structures. *Struct. Des. Tall Spec. Build.* **2022**, e1967. [[CrossRef](#)]

38. Ghannadi, P.; Kourehli, S.S.; Noori, M.; Altabay, W.A. Efficiency of grey wolf optimization algorithm for damage detection of skeletal structures via expanded mode shapes. *Adv. Struct. Eng.* **2020**, *23*, 2850–2865. [CrossRef]
39. Ghannadi, P.; Kourehli, S.S. Multiverse optimizer for structural damage detection: Numerical study and experimental validation. *Struct. Des. Tall Spec. Build.* **2020**, *29*, e1777. [CrossRef]
40. Gomes, G.F.; Giovani, R.S. An efficient two-step damage identification method using sunflower optimization algorithm and mode shape curvature (MSDBI-SFO). *Eng. Comput.* **2020**, *38*, 1711–1730. [CrossRef]
41. Pereira, J.L.J.; Francisco, M.B.; Jr, S.S.d.C.; Gomes, G.F. A powerful Lichtenberg optimization algorithm: A damage identification case study. *Eng. Appl. Artif. Intell.* **2021**, *97*, 104055. [CrossRef]
42. Pereira, J.L.J.; Chuman, M.; Jr, S.S.C.; Gomes, G.F. Lichtenberg optimization algorithm applied to crack tip identification in thin plate-like structures. *Eng. Comput.* **2021**, *38*, 151–166. [CrossRef]
43. Khatir, S.; Tiachacht, S.; Thanh, C.L.; Tran-Ngoc, H.; Mirjalili, S.; Wahab, M.A. A robust FRF damage indicator combined with optimization techniques for damage assessment in complex truss structures. *Case Stud. Constr. Mater.* **2022**, *17*, e01197. [CrossRef]
44. Tran-Ngoc, H.; Khatir, S.; Le-Xuan, T.; Tran-Viet, H.; Bui-Tien, T.; De Roeck, G.; Wahab, M. A. Damage assessment in structures using artificial neural network working and a hybrid stochastic optimization. *Sci. Rep.* **2022**, *12*, 1–12. [CrossRef] [PubMed]
45. Minh, H.-L.; Khatir, S.; Rao, R.V.; Wahab, M.A.; Cuong-Le, T. A variable velocity strategy particle swarm optimization algorithm (VVS-PSO) for damage assessment in structures. *Eng. Comput.* **2021**. [CrossRef]
46. To, T.S.; Le, M.H.; Danh, T.T.; Khatir, S.; Abdel Wahab, M.; Le, T.C. Combination of intermittent search strategy and an Improve Particle Swarm Optimization algorithm (IPSO) for model updating. *Frat. Ed Integrità Strutt.* **2022**, *59*, 141–152.
47. Kaveh, A.; Akbari, H.; Hosseini, S.M. Plasma generation optimization: A new physically-based metaheuristic algorithm for solving constrained optimization problems. *Eng. Comput.* **2020**, *38*, 1554–1606. [CrossRef]
48. Kaveh, A.; Vaez, S.R.H.; Hosseini, P.; Fallah, N. Detection of damage in truss structures using Simplified Dolphin Echolocation algorithm based on modal data. *Smart Struct. Syst.* **2016**, *18*, 983–1004. [CrossRef]
49. Kaveh, A.; Hosseini, S.M.; Zaeerza, A. boundary strategy for optimization-based structural damage detection problem using metaheuristic algorithms. *Period. Polytech. Civ. Eng.* **2020**, *65*, 150–167. [CrossRef]
50. Mohebian, P.; Aval, S.B.B.; Noori, M.; Lu, N.; Altabay, W.A. Visible particle series search algorithm and its application in structural damage identification. *Sensors* **2022**, *22*, 1275. [CrossRef]
51. Aval, S.B.B.; Mohebian, P. Joint damage identification in frame structures by integrating a new damage index with equilibrium optimizer algorithm. *Int. J. Struct. Stab. Dyn.* **2022**, *22*, 2250056. [CrossRef]
52. Aval, S.B.B.; Mohebian, P. A novel optimization algorithm based on modal force information for structural damage identification. *Int. J. Struct. Stab. Dyn.* **2021**, *21*, 2150100. [CrossRef]
53. Ahmadianfar, I.; Bozorg-Haddad, O.; Chu, X. Gradient-based optimizer: A new metaheuristic optimization algorithm. *Inf. Sci.* **2020**, *540*, 131–159. [CrossRef]
54. Li, J.; Gao, Y.; Zhang, H.; Yang, Q. Self-adaptive opposition-based differential evolution with subpopulation strategy for numerical and engineering optimization problems. *Complex Intell. Syst.* **2022**, *8*, 2051–2089. [CrossRef]
55. Wang, W.-C.; Xu, L.; Chau, K.-W.; Zhao, Y.; Xu, D.-M. An orthogonal opposition-based-learning Yin–Yang-pair optimization algorithm for engineering optimization. *Eng. Comput.* **2021**, *38*, 1149–1183. [CrossRef]
56. Clerc, M.; Kennedy, J. The particle swarm-explosion, stability and convergence in a multidimensional complex space. *IEEE Trans. Evol. Comput.* **2002**, *6*, 58–73. [CrossRef]
57. Tsai, H.C. Unified particle swarm delivers high efficiency to particle swarm optimization. *Appl. Soft Comput.* **2017**, *55*, 371–383. [CrossRef]
58. Wu, G.; Mallipeddi, R.; Suganthan, P.N. *Problem Definitions and Evaluation Criteria for the CEC 2017 Competition and Special Session on Constrained Single Objective Real-Parameter Optimization*; Technical Report; National University of Defense Technology: Changsha, China; Kyungpook National University: Daegu, Republic of Korea; Nanyang Technological University: Singapore, 20 September 2017.
59. Suganthan, P.N. Available online: <https://github.com/P-N-Suganthan/2020-RW-Constrained-Optimisation> (accessed on 15 July 2022).
60. Mirjalili, S.; Mirjalili, S.M.; Lewis, A. Grey wolf optimizer. *Adv. Eng. Softw.* **2014**, *69*, 46–61. [CrossRef]
61. Mirjalili, S.; Lewis, A. The whale optimization algorithm. *Adv. Eng. Softw.* **2016**, *95*, 51–67. [CrossRef]
62. Mirjalili, S.; Mirjalili, S.M.; Hatamlou, A. Multi-verse optimizer: A nature-inspired algorithm for global optimization. *Neural Comput. Appl.* **2016**, *27*, 495–513. [CrossRef]
63. Mirjalili, S. SCA: A Sine Cosine Algorithm for solving optimization problems. *Knowl.-Based Syst.* **2016**, *96*, 120–133. [CrossRef]
64. Abualigah, L.; Diabat, A.; Mirjalili, S.; Elaziz, M.; Gandomi, A.H. The arithmetic optimization algorithm. *Comput. Methods Appl. Mech. Eng.* **2021**, *376*, 113609. [CrossRef]
65. Faramarzi, A.; Heidarinejad, M.; Stephens, B.; Mirjalili, S. Equilibrium optimizer: A novel optimization algorithm ☆. *Knowl.-Based Syst.* **2020**, *191*, 105190. [CrossRef]
66. Abualigah, L.; Yousri, D.; Elaziz, M.A.; Ewees, A.A.; Al-Qaness, M.A.A.; Gandomi, A.H. Aquila Optimizer: A novel metaheuristic optimization algorithm. *Comput. Ind. Eng.* **2021**, *157*, 107250. [CrossRef]

- 
67. Johnson, E.A.; Lam, H.F.; Katafygiotis, L.S.; Beck, J.L. Phase II of the ASCE benchmark study on SHM. In Proceedings of the 15th ASCE Engineering Mechanics Conference, New York, NY, USA, 2–5 June 2002.
  68. Johnson, E.A.; Lam, H.F.; Katafygiotis, L.S.; Beck, J.L. Phase I IASC-ASCE structural health monitoring benchmark problem using simulated data. *J. Eng. Mech.* **2004**, *130*, 3–15. [[CrossRef](#)]